SLAC-PUB-2858
December 1981
(T/E)

MULTIJET DECAYS OF QUARKONIA: TESTING THE THREE-GLUON VERTEX *

K. Koller and K. H. Streng
Institut für Theoretische Physik, Universität München

T. F. Walsh
DESY, Hamburg§ and CERN, Geneva

P. M. Zerwas¶
Stanford Linear Accelerator Center
Stanford University, Stanford, California 94305

ABSTRACT

We study the 4 jet and photon plus 3 jet decays of orthoquarkonia,

$$^3S_1(Q\bar{Q}) \to GGGG + GGq\bar{q} \to 4 \text{ jets}$$

$$^3S_1(Q\bar{Q}) \to \gamma GGG + \gamma Gq\bar{q} \to \gamma + 3 \text{ jets} \quad .$$

We show that the characteristic features of the jet distributions in the final state are determined by the 3-gluon vertex of quantum chromodynamics. These decays of a heavy quarkonium resonance (toponium) will offer clear signals for the gluons' self-coupling which can establish QCD as a local non-Abelian gauge theory.

Submitted to Nuclear Physics B

---

* Work supported in part by the Department of Energy, contract number DE-AC03-76SF00515, and in part by the Kade Foundation.
§ Permanent address, after 1 December 1981.
¶ Kade Foundation Fellow, on leave from Technische Hochschule Aachen.

1. Introduction

Short distance processes in quantum chromodynamics create partons—quarks and gluons. If all relevant distances are small, these partons have large momenta (of order the inverse distance) and are well separated in momentum space. Partons do not appear at large distances $\gtrsim 10^{-13}$ cm, but jets of hadrons do. If the jets are narrow and well enough separated in momentum space to be resolved, they tell us the energy and angle distribution the partons had at short distance. (Of course, there will be the fluctuations from the confinement process which makes a jet, so that the original parton momenta cannot be precisely defined. This smearing is less important the higher the momentum.)

Through parton distributions at short distances we can check that QCD is a local gauge theory with colored spinor quarks and colored vector gluons with a self-interaction [1]. That is the aim of the present paper. We look at parton or jet distributions in the decay of the spin 1, odd charge conjugation quarkonia ($J/\Psi, \Upsilon$, $(t\bar{t})$?) which can be produced in e^+e^- annihilation. In lowest order this decay is $(Q\bar{Q}) \to GGG \to 3$ jets or $(Q\bar{Q}) \to \gamma GG \to \gamma + 2$ jets [2]. In higher orders there will be radiative corrections to these processes and also more jets will appear. We consider (figs. 1 and 2)

$$\begin{aligned} (Q\bar{Q}) &\to GGGG \to 4 \text{ jets} \\ &\to GGq\bar{q} \to 4 \text{ jets} \end{aligned} \tag{1}$$

and

$$\begin{aligned} (Q\bar{Q}) &\to \gamma GGG \to \gamma + 3 \text{ jets} \\ &\to \gamma Gq\bar{q} \to \gamma + 3 \text{ jets} \quad . \end{aligned} \tag{2}$$

The parton or resolved jet distributions in these higher order decays depend on the 3-gluon vertex of QCD, and comparing our predictions to experiment will allow one to confirm (or refute) its presence. (We previously studied $C = +$ $(Q\bar{Q})$ decays as a prelude [3]; see also ref. 4.) We intend for this to be done on the $^3S_1(t\bar{t})$ resonance when it is found. Quarkonium decays are particularly useful for this test as to leading order the only partons created are gluons.

The T decays are well described by the QCD mechanism $(b\bar{b}) \to GGG \to$ 3 low energy jets [5]. Though clean jets are not seen, hadron distributions do need a matrix element containing vector gluons with color [6]. The next resonance should give very clean multijet decays, as there is clear evidence for an occasional third jet in $e^+e^- \to q\bar{q} + q\bar{q}G \to$ 2 jets + 3 jets at $E_{c.m.} \simeq 30$ GeV [7]. We thus take it as an empirical fact that at high energy partons at short distances give narrow jets, and that we can study the angle and energy distributions of partons in (1) and (2) by studying their jets. The fact that 3 jet events in e^+e^- are only $\sim 20\%$ of the total rate supports our view that (1) and (2) can also be treated perturbatively, to order g_s^4 and eg_s^3 respectively. The mean number of resolvable jets should increase only slowly with energy, so that our perturbative calculation will be adequate up to $(t\bar{t})$ masses of 40-80 GeV. An important step in proving that radiative corrections do not disrupt low order phenomenology for $^3S_1(Q\bar{Q})$ decays is the calculation of the total rate by Mackenzie and Lepage [8] up to order g_s^8. The rate corrections are in fact controllable.

Since the jet resolution is crucial for the tests we propose, we discuss some more details of this problem in the next section.

In section 3 we present the 4 jet analysis of $(Q\bar{Q}) \to GGGG$ and $GGq\bar{q}$. We consider the kinematics, and the results of our calculations are illustrated by various distributions, including jet energies and angular correlations between the jets. The analysis is repeated in section 4 for photonic decays $(Q\bar{Q}) \to \gamma GGG$ and $\gamma Gq\bar{q}$. All these decays, when observed on a heavy $(t\bar{t})$ resonance, offer a clean laboratory to study gluon interactions. A short summary of some of our results has appeared previously [9].

2. Jet Resolution in QCD

Tests of the sort we propose will clearly not work easily if the confinement process of jet formation is too intertwined with the perturbative generation of partons. There is evidence that the two can be separated at present energies. As an example, the simplest (and, of course, incomplete) approach to $e^+e^- \to q\bar{q} + q\bar{q}G \to 2$ jets + 3 jets (neglecting further radiative corrections, or neglecting yet higher orders in g_s) is the following [10]. In $q\bar{q}G$, if the invariant mass of (qG) or $(\bar{q}G)$ is below some cutoff $\sqrt{p^2_{NP}}$, the event is taken to contain two partons only, $q\bar{q}$. If the invariant mass is above this cutoff, three partons are present — $q\bar{q}G$. The (qG) or $(\bar{q}G)$ parton mass cutoff can be chosen to be from 5-7 GeV, on the grounds that above this value individual qG or $\bar{q}G$ jets can be distinguished as for $e^+e^- \to q\bar{q} \to 2$ jets at SPEAR energies. (This evidently just uses the most naive operational discrimination between a two and a three jet event.) Finally, each parton is independently replaced by a jet of hadrons. This parametrizes confinement in a simple way. The procedure accounts for data astonishingly well [7]. The presence of a (qG) or $(\bar{q}G)$ mass cutoff is of course

irrelevant when only clean three jet events are studied, as all pair invariant masses can then be chosen large.

We can compare this simple procedure to a more sophisticated one, due to the Lund group [11]. They account carefully for the low momentum hadrons, rather than superimposing independent jets, and they also model the nonperturbative color flow in gluon fragmentation. Their model thus interpolates smoothly between two and three jet regimes. Comparing the two approaches to the data [12], the differences turn out to be rather subtle at present energies. If one is only interested in modelling the confinement fluctuations and the smearing of parton energies and angles, the simplest procedure is good enough. This is hardly surprising, as we are interested in essentially calorimetric quantities which ought to be insensitive to the details of confinement. For our purposes here, it is acceptable to replace partons by jets generated in the familiar way.

Eventually one would like to do better than this. But we want to add a cautionary remark. Static QCD properties on a lattice show a rather abrupt transition from the weak coupling regime to the strong coupling regime [13]. Jet formation is a dynamic process and there is no comparable understanding of it. But it is at least not excluded that there is a similarly sudden transition from the perturbative to the nonperturbative regime. Maybe it is not possible to follow parton evolution below some critical invariant mass. We think that tests such as ours must not depend critically on the evolution of low mass partons (e.g., $\sqrt{p^2} \lesssim$ 5-7 GeV at present energies). The available evidence appears to support our view that there is an insensitivity to this kinematic regime [12].

There is some evidence that QCD radiative corrections to multijet events can be dealt with similarly. Consider the QED processes $e^+e^- \to \mu^+ + \mu^- + \gamma$ and $e^+e^- \to (\mu^+ + \text{soft or collinear } \gamma) + \mu^- + \gamma$. Because of detector resolution, the two must be combined for small enough $[p_{\mu^+} + p_\gamma \text{ (soft/coll)}]^2 \lesssim \mu^2$. Similarly, a radiative $e^+e^- \to q + \bar{q} + G$ must be combined with $e^+e^- \to (q + \text{soft/coll } G) + \bar{q} + G$. In QCD one can attempt to extend the operational rule we gave for $e^+e^- \to q\bar{q} + q\bar{q}G$ so as to include radiative corrections to $q\bar{q}G$. Consider noncollinear events through the next orders in g_s, $q\bar{q}G + q\bar{q}GG + q\bar{q}q\bar{q}$ ($q\bar{q}G$ now contains loop corrections). When two and only two of the four partons have low invariant mass $p^2 \lesssim p^2_{NP}$, the state can be uniquely combined with $q\bar{q}G$. For very soft gluons the pairing with smallest p^2 can be chosen, or one can make a calculationally convenient choice. (The resulting cross section must of course be finite, with loop and soft divergences cancelling one another.) This provides us with an operational definition of a radiatively corrected 3 jet rate: loop corrections plus those 4 parton configurations which mimic 3 parton ones after a cutoff p^2_{NP}. (Of course, the perturbative result depends on this cutoff in a well-defined way. The situation is not so unfamiliar in the context of QED tests.) The remaining events have 4 jets—as yet not radiatively corrected.

The cutoff we describe is only partly set by detector resolution. Most of it is due to confinement. A collection of hadrons roughly collimated in angle cannot have a very low invariant mass. This p^2_{NP} can be chosen to be the mass of a typical jet, $\sqrt{p^2_{NP}} \sim 5$ GeV at present Q^2. (How very soft particles in the lab are assigned to jets

won't change $\sqrt{p_{NP}^2}$ much.) The exact numerical value of p_{NP}^2 essentially sets the scale at which one first resolves 3 jets in e^+e^- annihilation.

The radiative corrections to $q\bar{q}G$ have been cast in this form by Kunszt [14] based on work in refs. 15 and 16. He shows that the shape of the 3 jet distributions defined this way agree reasonably with the lowest order Born approximation distributions. The total radiatively corrected 3 jet rate up to this order can be obtained in a simple approximate way. One just replaces the coefficient of the Born cross section, $\alpha_{LO}(Q^2) \to \alpha_{LO}[(p_q + p_G)^2 (p_{\bar{q}} + p_G)^2 / Q^2]$, where α_{LO} is the lowest order one loop coupling and the scale parameter in the right hand side is now the true $\Lambda_{\overline{MS}}$. The change in the dimensional scale in α_{LO} is not amazing, since the "distance" involved in the coupling is not actually $1/\sqrt{Q^2}$ but some larger value, related to the mean invariant mass of paired partons.

One can as well carry out this sort of analysis using other variables [17]. It is probably even desirable to do so, since in this way one can get a better practical understanding of the problem.

There is no general proof that the above procedure works to all orders for $e^+e^- \to$ multijets, let alone that it is valid for all other processes such as (1) and (2)。 Yet it is physically a very simple prescription: the radiative corrections can mostly be accounted for by a change in the dimensional scale in α_s, and by a definition of a jet mass (or by some other appropriate definition of a jet). The remaining corrections are hopefully then truly small enough to ignore. We conjecture that this is in fact general and that radiative corrections and confinement effects are both controllable when handled in the way we have described. In fact, this conjecture is nicely supported for $^3S_1(Q\bar{Q})$

decays by the calculation of Mackenzie and Lepage [8] proving that the rate corrections are in fact controllably small. The same conclusion can be drawn from the radiative corrections of heavy paronium decays in ref. 18.

In the following we will proceed to discuss higher order jet distributions in orthonium decay without further detailed discussion of these points. A quantitative estimate of the confinement fluctuations in jet energies and angles relative to parton variables is simply obtained by using our matrix elements as input to a jet generating routine.

3. Four-Jet Decays of Orthonium

3.1 GENERALITIES

The decay amplitude of a heavy $^3S_1(Q\bar{Q})$ state to some final state F in the static approximation is

$$\mathcal{T} = \frac{1}{\sqrt{2}} \operatorname{tr}\left\{ \mathcal{M}\,(1+\gamma^0)\; \not{\epsilon}(S_z) \right\} \Phi(0) \qquad (3)$$

where $\mathcal{M}$ is the $Q\bar{Q} \to F$ Feynman amplitude without external spinors, Φ is the usual nonrelativistic wavefunction at the origin and $\epsilon_\mu(S_z)$ is the $(Q\bar{Q})$ polarization vector for spin component S_z (fig. 3). In this approximation, the mass of the bound state is $M = 2m_Q = 2E_B$ (E_B is the beam energy in e^+e^-). Except where explicitly stated we use units of the beam energy, so $M = 2$.

We ignore internal motion and also higher order radiative corrections to the 4 jet distributions. The former will have only a very small effect on jet distributions. We explained in the preceding section why we think that radiative corrections are controllable.

A more pessimistic point of view would be that they could unpredictably affect distributions at the 0(20%) level. This is too small to affect our conclusions. We will see that the effects of the 3G vertex are dramatic, and are not just of order 20%.

The matrix elements for $(Q\bar{Q}) \to GGGG$ (labelled by colors $a_1\, a_2\, a_3\, a_4$) are proportional to products of color SU(3) f and d tensors. The overall color factors depend on the type of diagram in fig. 1.

When all gluon lines are attached by the heavy quark line we have (fig. 1a) a factor

$$\frac{i}{8\sqrt{3}} \sum_m \left[f_{a_1 a_2 m} d_{m a_3 a_4} + d_{a_1 a_2 m} f_{m a_3 a_4} \right] \quad .$$

For the diagram with a 3G vertex at the bottom in fig.1b, there is a factor

$$\frac{i}{4\sqrt{3}} \sum_m d_{a_1 a_2 m} f_{m a_3 a_4} \quad .$$

The amplitude for $(Q\bar{Q}) \to GGq\bar{q}$ with colors a_1, a_2 and i,j contains a factor

$$\frac{1}{8\sqrt{3}} \sum_m d_{a_1 a_2 m} \left(\lambda^m\right)_{ij} \quad .$$

It is useful to realize that when the matrix element is squared and summed over color indices a_i only a few products of

$$C^{\pm}_{a_1 a_2 a_3 a_4} = \sum_m \left[f_{a_1 a_2 m} d_{m a_3 a_4} \pm d_{a_1 a_2 m} f_{m a_3 a_4} \right] \qquad (4)$$

do not vanish. They are

$$
\begin{aligned}
\sum C^{+}_{a_1a_2a_3a_4}\, C^{+}_{a_1a_2a_3a_4} &= 80 \\
\sum C^{+}_{a_1a_2a_3a_4}\, C^{+}_{a_1a_4a_3a_2} &= -80 \\
\sum C^{-}_{a_1a_2a_3a_4}\, C^{-}_{a_1a_2a_3a_4} &= 80 \\
\sum C^{-}_{a_1a_2a_3a_4}\, C^{-}_{a_1a_3a_2a_4} &= -80 \\
\sum C^{-}_{a_1a_2a_3a_4}\, C^{+}_{a_1a_2a_4a_3} &= 80 \\
\sum C^{-}_{a_1a_2a_3a_4}\, C^{+}_{a_1a_3a_4a_2} &= -80
\end{aligned}
\qquad (5)
$$

together with those obtained by interchanging $a_1a_2 \leftrightarrow a_3a_4$ and so on.

The Feynman amplitudes for the four parton final state were calculated in the axial gauge with $n_\mu = Q_\mu$, i.e., assuming transverse gluon polarization (see the Appendix). Squared and summed over polarizations and color factors, these give the decay rates for an unpolarized $(Q\bar{Q})$ state. Angular correlations of jets with the e^+e^- beams can be calculated by taking appropriate initial state polarization amplitudes.

Assuming that the intial $(Q\bar{Q})$ state is unpolarized (or that the lab orientation of the 4 jet state is averaged over), the final state can be characterized by the following variables. (1) The lab energy of one jet (jet 1) x_1, expressed in units of the beam energy. (2) The energy of a second jet (jet 2) in the rest frame of the three jet system recoiling against jet 1, x_2^R. Similarly for x_3^R. The unit for these variables is half the recoil mass $\sqrt{1 - x_1}$ (not the beam energy).

(3) The polar angle θ^R of jet 2 with respect to the direction of jet 1 in the recoil rest frame. (4) The azimuthal angle ϕ^R between the x_1, x_2^R and x_3^R, x_4^R plane, also taken in the recoil rest frame.

In units of the lowest order 3-gluon rate

$$\Gamma_{LO} = \frac{40}{81} \alpha_s^3 \left(\pi^2 - 9\right) \frac{|\Phi(0)|^2}{m_Q^2} \tag{6}$$

the partial decay rate is

$$\frac{1}{\Gamma_{LO}} \frac{d\Gamma(4 \text{ jets})}{dx_1\, dx_2^R\, dx_3^R\, d\cos\theta^R\, d\phi^R} = \frac{\alpha_s}{\pi} \frac{81}{40\left(\pi^2 - 9\right)} \frac{x_1\left(1 - x_1\right)}{4\pi S} |\mathscr{T}|^2 \tag{7}$$

where the statistical factor S is 4! for 4 gluon final states and 2! for $GGq\bar{q}$. An average over initial $(Q\bar{Q})$ polarizations is assumed.

Sometimes it is useful to characterize a 4 jet configuration by the four jet energies x_i in the lab $(\sum x_i = 2)$, the momentum x_{12} of a pair of jets $(x_{12}^2 = x_1^2 + x_2^2 + 2x_1x_2\cos\theta_{12})$ and the azimuthal angle φ between the x_1, x_2 and x_3, x_4 plane. The phase space element related to this configuration is $d\mathscr{R} = (\pi^2/2)\, d\varphi\, dx_1\, dx_2\, dx_3\, dx_{12}$.

We want to preface our detailed discussion by some general remarks on the various amplitudes in figs. 1a, 1b and 1c. First we note that in an Abelian theory $(Q\bar{Q})$ cannot decay to 4-gluons at all. Only $GGq\bar{q}$ is allowed. Second, we calculate helicity amplitudes. It is thus possible to separate the contribution which involves the 3G vertex (fig. 1b) from that which does not (fig. 1a). For transverse gluons in the final state there is no gauge dependence which might mix these two diagrams. This allows us to isolate the effects of the 3-gluon vertex in all our distributions. We do this because it is obviously vital to check experimentally the existence of all the terms in the QCD Lagrangian. Our expectations for (1) and (2) are backed up by an analysis of S-wave

paronium decays to three jets [3]. As in that case, we will find that the amplitudes of fig. 1a are very small and that fig. 1b dominates over 1c, even for five "light" quark flavors. The 3G vertex is indeed very important in quarkonium decays.

The contributions from diagrams 1a, 1b and 1c are quite different when one of the final state quanta is soft or two of them are collinear. This produces a hierarchy between the different diagrams. The diagrams where all gluons are attached to the heavy fermion line is finite everywhere for S-wave $(Q\bar{Q})$ decays. Propagator divergences are cancelled by a vanishing amplitude for a heavy quark at rest to radiate a zero energy transverse gluon [19]. By contrast, the diagram including the 3G vertex $G \to GG$ shows a typical bremsstrahlung character, in close analogy to the bremsstrahlung of a gluon by a quark, $q \to qG$. In these cases the radiated vector quantum has an energy and transverse momentum distribution $dN \propto dE/E \cdot dp_T^2/p_T^2$, at small E and p_T^2. On the other hand, gluon splitting into a quark-antiquark pair is infrared finite but singular for collinear configurations, $dN \propto dE \cdot dp_T^2/p_T^2$. Thus $G \to GG$ will dominate over $G \to q\bar{q}$ (which also occurs in Abelian theories), and amplitudes where all gluons are radiated by a heavy fermion are negligible compared to these. We thus expect that distributions are dominated by the gluons' self-coupling. For this reason, the evolution of single particle spectra (or, rather, their moments) from one onium state to the next can be calculated [20] from Altarelli-Parisi type equations [21].

The last qualitative point we wish to emphasize is the overall normalization. From $(Q\bar{Q}) \to 3G$ or $e^+e^- \to q\bar{q}G$ we can regard the normalization of the $q\bar{q}G$ vertex as fixed, up to the logarithmic dependence

of α_s. Thus the $(Q\bar{Q}) \to GGq\bar{q}$ rate is fixed by processes which have already been observed. The overall $(Q\bar{Q}) \to 4$ jet rate then provides a measure of the importance of the 3G vertex contribution of this process —independent of the precise shape of the distributions. For realistic cuts on parton invariant masses, we will see that the overall rate is about four times the "known" $(Q\bar{Q}) \to GGq\bar{q}$ rate (we use five "light" quark flavors).

3.2 DISTRIBUTIONS

Distributions will, or course, be affected by the cut which has to be introduced to make sure that we can speak of a 4-parton state. In units of the beam energy we will choose a cut on parton pair masses $m_{ij} \geq m_{cut}$ with $m_{cut} = 2/9$ (corresponding to a 5 GeV mass cut for a 45 GeV mass onium state). We will occasionally use a smaller cut so as to illustrate the qualitative behavior in more detail.

In order to make the cut dependence clear, we show in fig. 4 the total Γ_4 as a function of m_{cut}, normalized to α_s/π. For $m_{cut} = 2/9$ we find a total 4-jet rate 13 α_s/π times the lowest order rate. This is probably near the maximum one can tolerate without making a calculation of the 5-parton final state necessary.* This figure clearly shows the dominance of the four-gluon final state over $GGq\bar{q}$, and also that the four-gluon final state is dominated by the three-gluon vertex for massless transverse gluons. Thus we expect that the 3-jet topology will be dominant in quarkonium decays, with a significant number of 4-jet events.

---

*The magnitude of the cross section for this mass cut is typical for other bremsstrahlung processes as $0^{-+} \to GGG$ [3] and $e^+e^- \to q\bar{q}GG/q\bar{q}G$.

(Events with more than four jets or events from hadronic weak decays of the t quark can be separated out and analyzed by themselves. We imagine that this separation is obtained through some kind of cluster analysis for jets [22]. Our remarks which follow apply to the 4-jet class of events.)

To show the general features related to the 3G vertex, we first look into the distribution of the invariant masses of all quark and gluon pairs in the final state. The distribution most sensitive to soft and collinear singularities will be the minimum parton pair mass

$$m_{MIN} = \min\left(m_{ij}\right) \tag{8}$$

where $m_{ij}^2 = (p_i + p_j)^2$ with p_i the parton four momenta (i,j = 1,2,3,4). The kinematic limits of this variable are (the upper limit corresponds to the symmetrical pyramid configuration)

$$m_{cut} \leq m_{MIN} \leq \sqrt{\frac{2}{3}} \tag{9}$$

and fig. 5 shows

$$\frac{1}{\Gamma_{LO}} \frac{d\Gamma}{dm_{MIN}} \quad .$$

We note that the contribution of fig. 1a is totally negligible, as already mentioned. The contribution of the 3G vertex to $(Q\bar{Q}) \rightarrow GGGG$ exceeds $(Q\bar{Q}) \rightarrow GGq\bar{q}$ by a factor ~ 4 at the lowest m_{MIN} and by less at higher values of this variable. Lowering m_{cut} would increase the fraction of events due to the 3G vertex. (This would be relevant in considering the inclusive particle distribution on successive onium states.)

The bremsstrahlung character of the dominant decay modes is also reflected in the classical measure of the acoplanarity of the events.

This is demonstrated by the minor distribution in fig. 6. Naturally, $G \to GG$ induces a sharp rise of the distribution near zero. This rise is an order of magnitude stronger than in the 4-gluon decay without 3G vertex which sets the scale of phase space effects involved.

An important distinction between $G \to q\bar{q}$ and $G \to GG$ distributions follows from our earlier remarks. Consider the energy difference between the two partons paired in the 2-jet bundle of minimum invariant mass. The spectrum of gluons radiated by a (nearly real) gluon has a z^{-1} bremsstrahlung singularity [21]

$$D_{G\to G}(z) = 6 \frac{\left(1 - z + z^2\right)^2}{z(1-z)} \tag{10}$$

(where z is the fractional energy transferred from the initial to a final gluon). As a consequence of this infrared singularity for $z \to 0$ or 1, the energy distribution among the final gluons is asymmetric. This gives an increase of the distribution of the difference $\Delta x = |x_i - x_j|$ towards 1. (x_i and x_j are the energies of the jets or partons making up the minimum invariant mass 2-jet bundle.) By contrast, gluon splitting into quark and antiquark does not have this behavior, since

$$D_{G\to q}(z) = \frac{N_F}{2}\left[z^2 + (1-z)^2\right] . \tag{11}$$

The resulting spectrum is rather flat.

In fig. 7a, we show the distribution

$$\frac{1}{\Gamma_4} \frac{d\Gamma_4}{d\Delta x}$$

for a cut $m_{cut} = 1/9$. It is plausible that the mass cuts eliminate events with large Δx, but a pronounced difference between the shapes of

Δx distributions for 4G and $GGq\bar{q}$ final states persists. This is even so if the minimum parton pair mass is constrained to $2/9 \leq m_{MIN} \leq 3/9$ as shown in fig. 7b. The bremsstrahlung asymmetry therefore offers a unique test of the 3-gluon coupling.

3.3 CLASS A AND CLASS B EVENTS

The 4-jet events fall into two classes when analyzed in terms of thrust [23]. In the first class the thrust axis is the axis of a jet, with three jets on the other side of a plane perpendicular to the axis. We call these class A (fig. 8a). The other class is made up of events where there are two jets on each side of a plane perpendicular to the thrust axis (which lies along the sum of the momenta of the two jets in each hemisphere). We call these class B (fig. 8b).

There are many distributions which are most useful when examined separately for class A and class B events. As is clear from table 1, the fractions are both large for a reasonable range of m_{cut}. For very small values of m_{cut} the fraction of class A events goes to zero, as does the fraction of $GGq\bar{q}$ events. Both these effects are due to the gluon bremsstrahlung via $G \rightarrow GG$.

Class A events are best parametrized by the energy of the fastest jet, and the energies and orientation of the three recoiling jets in their c.m. frame. Class B events, on the other hand, should be characterized by the energies of the jets, the sum x_{ij} of the momenta of, say, the 2-jet bundle with minimal mass, and the angle between the two planes formed by i,j and the two remaining jets.

Class A Events. As we mentioned before, these events have the thrust axis along a jet momentum vector (fig. 8a). For our value of $m_{cut} = 2/9$ approximately 30% of the 4 jet events fall into this class. These events are useful because one can boost into the rest frame of the three recoiling jets in a unique way. Four independent energy and angle distributions in this frame can be studied in the same way as $e^+e^- \to q\bar{q}G \to 3$ jets.

Consider the thrust distribution (distribution of the energy of the most energetic jet) in this rest frame. The distribution of

$$\frac{1}{\Gamma_{LO}} \frac{d\Gamma_4}{dT_R}$$

is shown in fig. 9, where T_R is the recoil rest frame thrust.* Note that the thrust distribution for pure gluon final states is larger than for $G\bar{q}q$, and it falls off more rapidly towards low T_R. This steeper dependence of the gluon final state is due to the bremsstrahlung behavior of $G \to GG$.

We can again look into the energy asymmetry of the two softer jets in the 3-jet recoil rest frame. We find that, similarly to fig. 7, the average energy difference in gluon final states is larger than in quark-antiquark final states.

The development of the event topology in the recoil system parallels the development in the e^+e^- continuum. At low invariant recoil mass, the hadrons form two slim jets (mainly gluon jets) which quickly broaden with

---

* This variable is now normalized to half the recoil mass, $\sqrt{1-x_1}$, so $2/3 \leq T_R \leq 1$ for $m_{cut} = 0$.

rising mass. For large recoil masses, clear three-jet structures can finally be resolved. Due to the integer color change of gluons, this multijet structure develops faster in gluon final states of quarkonia than in quark final states of the continuum. These points will be elaborated in greater detail for γ decays of quarkonia.

There are other potentially interesting distributions — above all, the orientation of the recoil 3 jet system in space. The T_R thrust axis is expected to be aligned predominantly along the main thrust axis for 4G final states, whereas the azimuthal distribution will be fairly flat. We have studied these distributions but will refrain from showing them. The main points we have to make are already clear from fig. 9.

Class B Events. A schematic class B event is shown in fig. 8b. The majority of 4-jet events belong to this class, $\geq 65\%$, independent of m_{cut}. We have selected three representative observables to demonstrate the effects of the 3G vertex.

The first is the energy of the thin two-jet bundle in its rest frame (equivalently, its invariant mass). This is shown in fig. 10. The shape of the distribution

$$\frac{1}{\Gamma_{LO}} \frac{d\Gamma_4}{dm_{ij}}$$

is different for GG in the thin jet compared to $q\bar{q}$ in the thin jet. (m_{ij} is the invariant mass of the 2 jet bundle.) By contrast the shape of the two contributions is quite similar in the fat jet bundle. This behavior is again due to the 3G vertex. Note the much steeper fall off of the 4G distribution compared to the $GGq\bar{q}$ final states in the slim 2-jet bundle.

Another characteristic distribution is presented in fig. 11. We define $\cos\theta_{ij}$ to be the cosine of the angle of the two jets in a bundle to the overall 4-jet thrust axis, defined in the rest frame of the 2-jet bundle.[§] For $G \to GG$ we expect this axis to lie along the overall 4-jet thrust axis — i.e., $|\cos\theta_{ij}| = 1$ is favored. For $G \to q\bar{q}$ a flatter distribution is expected. Figure 11 shows

$$\frac{1}{\Gamma_{LO}} \frac{d\Gamma_4}{d\cos\theta_{ij}}$$

for the thin 2-jet bundle ($2/9 \leq m_{MIN} \leq 3/9$ cut). We see a clear signature for $G \to GG$. (This is absent in the distribution of the same quantity for the fat 2-jet bundle.)

Other signals have been discussed as a check on the 3G vertex — for example, the azimuthal angular (χ) distribution of the G'G' or $q\bar{q}$ plane in

$$(Q\bar{Q}) \to GG + G^* \quad (12)$$
$$\qquad\qquad\quad \hookrightarrow G'G' \text{ and } q\bar{q}$$

defined relative to the GG plane [25]. This angular correlation is due to a partial linear polarization of G^* perpendicular to the GGG^* plane (for details see refs. 3, 26). In a straightforward generalization of (10) and (11) we expect for the distribution of the G'G' and $q\bar{q}$ plane in a slim 2-jet bundle, relative to the polarization vector of G^*,

---

§ This angular distribution is closely related to the distribution of the difference of the jet energies in the slim 2-jet bundle (lab frame); se also ref. 24.

$$D_{G\to G}(z,\chi) = \frac{6}{2\pi}\left\{\frac{\left(1-z+z^2\right)^2}{z(1-z)} + z(1-z)\cos 2\chi\right\} \qquad (13)$$

$$D_{G\to q}(z,\chi) = \frac{N_F}{2\pi}\left\{\frac{1}{2}\left[z^2+(1-z)^2\right] - z(1-z)\cos 2\chi\right\} \qquad (14)$$

In general, the G'G' plane tends to be perpendicular to the GG plane, whereas $q\bar{q}$ tends to lie in the same plane as GG. We have investigated the asymmetry for (12), defined as the number of events with azimuth between 0 and $\pi/4$ relative to the number with azimuth between $\pi/4$ and $\pi/2$ (normalized, of course, to the total number). This asymmetry — with our cuts on invariant masses of parton pairs — is of the order of a few percent, negative for 4G and positive for $q\bar{q}$, in agreement with (13) and (14). This is quite small. A similar asymmetry for events in the e^+e^- continuum has been discussed in ref. 23.

4. Photon Plus Three-Jet Decays

Heavy quarkonium decays $(Q\bar{Q}) \to \gamma$ + jets provide some important tests of quantum chromodynamics [2]. The radiative decay of J/ψ has been seen [27,28] but tests unimpeded by low energy effects, such as glueball production, will have to be carried out at more massive onia, Υ and $(t\bar{t})$. Toponium with its charge 2/3 quarks will be particularly useful. The Born approximation ratio

$$\frac{\Gamma_{LO}(\gamma GG)}{\Gamma_{LO}(GGG)} = \frac{36}{5}\,\frac{\alpha}{\alpha_s}\,e_Q^2 \approx 20\% \qquad (15)$$

is large enough for a detailed analysis of this decay channel. The direct photon decays have a clean signature that makes up for the lower rate compared to pure hadronic decays. There are other advantages. It filters out direct weak t quark decays, which become increasingly important as m_t

increases [29].* They will potentially disturb a 4-jet analysis above onium masses of about 75 GeV. The impact on γ decays will be much less. Another advantage is that radiative decays will show a better signal to background ratio than hadronic decays if there should be a large continuum contribution under a $(t\bar{t})$ peak.

For a resonance mass M of 40 to 75 GeV, the mass M_R of the hadronic recoil system against a photon can easily be tuned in the range between 10 and 40 or 75 GeV by varying the γ energy,

$$M_R^2 = \left[1 - \frac{E_\gamma}{\frac{M}{2}} \right] M^2 \quad .$$

This is the energy range where gluon bremsstrahlung from quarks clearly emerges in e^+e^- continuum events. Suppose we look at the $(Q\bar{Q}) \to \gamma$ + jets final state in the multijet rest frame. Initially low mass back-to-back GG jets should broaden quickly with increasing M_R. Finally, a clear 3-jet structure should be visible. Figure 12 parallels the gluon-jet development in $(Q\bar{Q}) \to \gamma$ + jets with the quark-jet development in the e^+e^- continuum.

The gluon bremsstrahlung spectrum from a gluon source is $\sim 6\,dz/z$ compared to $(4/3)\,dz/z$ for a quark source. We therefore expect that in lowest order the jets broaden faster on an onium resonance than they do in the continuum [30] at the same $M_R = \sqrt{s}$. As an example, this will reflect itself in a more rapid increase of the average transverse momentum of single particle spectra,

$$\left[\langle p_\perp^2 \rangle - \langle p_\perp^2 \rangle_{NP} \right]_{Q\bar{Q}} \sim \frac{9}{4} \left[\langle p_\perp^2 \rangle - \langle p_\perp^2 \rangle_{NP} \right]_{e^+e^-} \qquad (16)$$

---

* Note however that only $\mathcal{O}(20\%)$ of these weak $(t\bar{t})$ decays are purely hadronic.

($\langle p_\perp^2 \rangle_{NP}$ refers to the nonperturbative transverse momentum spread in a quark or gluon jet at low energy; both appear to be nearly equal.)

In the following we investigate 3-jet distributions in the recoil system. The 3-jet rate depends, as before, on the cut in parton pair masses which we use to define a "resolved" multijet event or multiparton event. We use the same cuts as applied to 4-jet events, including the photon. This is necessary as to localize the γ emission in the femto-universe [31]. The ratio of γ + 3-jet events to the lowest order γGG rate turns out to be almost identical to the ratio of 4-jets to the GGG rate. The average photon energy is about half the heavy quark mass if these cuts are applied, leaving us with an average recoil mass of $\langle M_R \rangle \sim \sqrt{1/2}\ M$, i.e., ~ 30 to 35 GeV for a 45 GeV resonance. The mass of the recoil system is therefore in a range where clear 3-jet structures in the e^+e^- continuum can be resolved.

The recoil thrust distribution of such events is shown in fig. 13. The pattern is the same as for 4-jet events: $G \to GG$ dominates over $G \to q\bar{q}$, and there is only a very small contribution from the diagram where 3-gluons emerge from a heavy fermion line. Figure 14 shows the distribution of $(1/\Gamma_{LO})\ d\Gamma_3 / d\Delta x^R$, the jet energy asymmetry of the two slow jets in the recoil rest frame. We might note that a very similar plot of data for $e^+e^- \to q\bar{q}G \to 3$ jets shows a significant difference between scalar and vector gluon distributions [24].

As a final remark, we again draw attention to the overall normalization of $\Gamma_{\gamma 3} / \Gamma^{\gamma}_{LO}$ for clearly resolved γ + 3 jet events. Just as in the case of the ratio Γ_4 / Γ_{LO}, it depends on the 3-gluon vertex in a nontrivial way and thus can provide supporting evidence for its presence, independent of the detailed shapes of the distributions. It might be

amusing to compare the experimental rates and distributions for $(Q\bar{Q}) \to \gamma + 3$ jets and $(Q\bar{Q}) \to 4$ jets directly by treating the photon as just another parton (an unconfined one, of course).

5. Summary

On physical grounds, one expects that toponium will be a good place to look for experimental evidence of the 3-gluon vertex of QCD. We have shown that this is indeed the case. The overall rate for $(Q\bar{Q}) \to GGGG + GGq\bar{q} \to 4$ jets is about four times larger than expected in using the "known" $Gq\bar{q}$ vertex for $GGq\bar{q}$ and the (negligible) contribution to GGGG where all gluons are radiated from the heavy fermion line. A number of 4-jet distributions clearly show the presence of a $G \to GG$ contribution. These features are all present even including a lower limit on parton-parton masses so as to obtain a 4-jet configuration. Distributions will differ quite dramatically from, for example, a 4-jet phase space model. This is clear in comparing the overall shapes of our distributions to those for GGGG final states where the (transverse) gluons are all radiated by the heavy fermion. These will be qualitatively similar to 4-body phase space, and do not even resemble the contributions from $G \to GG$.

Distributions containing the $G \to GG$ vertex do differ significantly from those containing $G \to q\bar{q}$. Thus, there is clear evidence for the gluon bremsstrahlung spectrum dz/z from $G \to GG$ which is the most direct consequence of the 3-gluon vertex.

The process $(Q\bar{Q}) \to (\gamma + GGG) + (\gamma + Gq\bar{q}) \to \gamma + 3$ jets is particularly nice. In the recoil hadron rest frame one can compare jet broadening to that in e^+e^- annihilation. Even a relatively crude measurement should show that at recoil mass $M_R \simeq \sqrt{Q^2_{e^+e^-}}$ around 20-40 GeV events consists

of a thinner jet and a broad jet which is appreciably wider than in e^+e^-. Some events will show a resolution of the broad jet into two subjets also as in e^+e^- annihilation. Rates are large, and the distributions are marked by the effect of $G \to GG$, in particular the jet energy asymmetry.

Another significant comparison will be between moments of hadron momentum distributions [20] in $T(9.46) = (b\bar{b})$ and $(t\bar{t})$. When they are carefully compared to the evolution of moments of hadron distributions in the continuum we can expect additional strong support for the pre-presence of a $G \to GG$ vertex. The evolution in Q^2 of such distributions also depends on the p^2 (or mass) evolution of partons. It will be quite interesting to study these effects.

There is, of course, a missing element in our analysis — toponium has not yet been found. We await its discovery.

ACKNOWLEDGEMENTS

T. Walsh thanks J. Prentki for the hospitality of the CERN theory group. P. Zerwas is grateful to S. Drell for the hospitality extended to him at SLAC, and to the Kade Foundation for financial support. He owes special thanks to J. Bjorken for an encouraging discussion at the beginning of this study.

References

1. H. Fritzsch, M. Gell-Mann and H. Leutwyler, Phys. Lett. B47 (1973) 365; H. D. Politzer, Phys. Rev. Lett. 30 (1973) 1346; D. J. Gross and F. Wilczek, Phys. Rev. D8 (1973) 3497; T. Appelquist and H. D. Politzer, Phys. Rev. D12 (1975) 1404; H. D. Politzer, Phys. Rep. 14 (1974) 129; V. A. Novikov et al., Phys. Rep. 41 (1978) 1.

2. K. Koller and T. F. Walsh, Phys. Lett. 72B (1977) 227 [E: 73B (1978) 504] and Nucl. Phys. B140 (1978) 449; T. DeGrand, Y. J. Ng and H.-H. Tye, Phys. Rev. D16 (1977) 3251; S. Brodsky et al., Phys. Lett. 73B (1978) 203; H. Fritzsch and K. Streng, Phys. Lett. 74B (1978) 90; K. Koller, H. Krasemann and T. F. Walsh, Z. Physik C1 (1979) 71.

3. K. Koller, K. H. Streng, T. F. Walsh and P. M. Zerwas, Nucl. Phys. B193 (1981) 61.

4. R. Barbieri, G. Curci, E. d'Emilio and E. Remiddi, Nucl. Phys. B154 (1979) 535; A. N. Kamal, J. Kodaira and T. Muta, SLAC-PUB-2725.

5. C. Berger et al., Phys. Lett. 82B (1979) 449; S. Brandt, Proc., Geneva Conf. (1979); H. Meyer, Proc., FNAL Lepton-Photon Symp. (1979); reports of the Bonn Lepton-Photon Symposium (1981).

6. K. Koller and H. Krasemann, Phys. Lett. 88B (1979) 119; T. F. Walsh and P. M. Zerwas, Phys. Lett. 93B (1980) 53.

7. R. Brandelik et al., Phys. Lett. 86B (1979) 243; D. P. Barber et al., Phys. Rev. Lett. 43 (1979) 830; C. Berger et al., Phys. Lett. 86B (1979) 418; W. Bartel et al., Phys. Lett. 91B (1980) 142.

8. P. B. Mackenzie and G. Peter Lepage, Cornell preprint CLNS/81-498.

9. P. M. Zerwas, Proc. of the 4th International Colloquium on Photon-Photon Interactions, Paris (1981).

10. P. Hoyer et al., Nucl. Phys. B161 (1979) 349; R. Odorico, Z. Physik C4 (1980) 113.

11. B. Andersson, C. Gustafson and C. Peterson, Z. Physik C1 (1979) 105; B. Andersson and C. Gustafson, Z. Physik C3 (1980) 223.

12. W. Bartel et al., Phys. Lett. 101B (1980) 129.

13. C. Callan, Phys. Rep. 67 (1981) 123.

14. Z. Kunszt, Phys. Lett. 99B (1981) 429.

15. A. Ali et al., Nucl. Phys. B167 (1980) 454.

16. R. K. Ellis et al., Nucl. Phys. B178 (1981) 421; J.A.M. Vermaseren et al., Nucl. Phys. B187 (1981) 301.

17. K. Fabricius et al., DESY preprint 81/035; S. Sharpe, preprint LBL-13018 (1981); T. Gottschalk, preprint CALT-68-862.

18. R. Barbieri, R. Gatto and E. Remiddi, CERN preprint TH 3144.

19. T. F. Walsh et al., in ref. 6.

20. K. Koller, T. F. Walsh and P. M. Zerwas, Phys. Lett. 82B (1979) 263.

21. G. Altarelli and G. Parisi, Nucl. Phys. B126 (1977) 298; J. F. Owens, Phys. Lett. 76B (1978) 85; T. Uematsu, Phys. Lett. 79B (1978) 97.

22. H. Daum, H. Meyer and J. Bürger, Z. Physik C8 (1981) 167; J. Dorfan, Z. Physik C7 (1981) 349.

23. J. G. Körner, G. Schierholz and J. Willrodt, Nucl. Phys. B185 (1981) 365.

24. J. Ellis and I. Karliner, Nucl. Phys. B148 (1979) 141.

25. S. Brodsky, T. DeGrand and R. Schwitters, Phys. Lett. 79B (1978) 225; A. Smilga and H. Vysotksky, preprint ITEP-12 (1979).

26. J. G. Körner and D. McKay, DESY preprint 80/121.

27. G. S. Abrams et al., Phys. Rev. Lett. 44 (1980) 114.

28. M. T. Ronan et al., Phys, Rev. Lett. 44 (1980) 367.

29. T. Goldman, Los Alamos preprint LA-UR-77-1607; I. Bigi and H. Krasemann, Z. Physik C7 (1981) 127; J. Kühn et al., München preprint.

30. K. Shizuya and S.-H. Tye, Phys. Rev. Lett. 41 (1978) 778, (E) 1195; M. B. Einhorn and B. G. Weeks, Nucl. Phys. B146 (1978) 445.

31. J. D. Bjorken, Proc., SLAC Summer Institute (1979).

Appendix

Helicity Amplitudes and Cross Sections

In this Appendix we should like to present some more details on the helicity amplitudes for 4-gluon final states in fig. 1. We give the complete decay probability for $GGq\bar{q}$ final states. Photon decay matrix elements coincide with these apart from simple color (and for probabilities) statistics factors.

Let us begin with the somewhat simpler set of diagrams involving the 3-gluon vertex. After separating off the color factors and coupling constants, defined in section 3, the remaining amplitude corresponding to fig. 1b is called $F_1(1234)$; the virtual gluon in the middle, $F_2(1234)$; and at the top, $F_3(1234)$. A common factor $4\sqrt{2}\ \Phi(0)$ is left out. The amplitudes depend on the momentum vectors k_i (energies x_i) and the polarization vectors ε_i and ε of the gluons and the decaying quarkonium state, respectively. (Read ε_i as the complex conjugate of the polarization vector in the following.) The quark mass m_Q is chosen to be unity. These are the amplitudes.

$$F_1(1234) = \frac{\frac{1}{2}(\ell_1\ell_3) + (x_3 - x_4)(\varepsilon_3\varepsilon_4)\left[-(\varepsilon_1\varepsilon_2)(\varepsilon k_1) + (\varepsilon\varepsilon_1)(\varepsilon_2 k_1)\right]}{D_1}$$

$$F_2(1234) = \frac{\frac{1}{2}(\ell_2\ell_3)}{D_2}$$

$$F_3(1234) = -F_1(4321) \quad .$$

The 4-vectors ℓ_i are defined as

$$\ell_1 = \Big[(\varepsilon\Sigma)(\varepsilon_2 k_1) + (\varepsilon k_1)(\varepsilon_2\Sigma) - (\varepsilon\varepsilon_2)(\Sigma k_1)\Big]\varepsilon_1 - (\varepsilon_1 \leftrightarrow k_1)$$
$$+ \Big[(\varepsilon\varepsilon_1)(\Sigma k_1) - (\varepsilon_1\Sigma)(\varepsilon k_1)\Big]\varepsilon_2 + \Big[(k_1\varepsilon_2)(\varepsilon_1\Sigma) - (\varepsilon_1\varepsilon_2)(k_1\Sigma)\Big]\varepsilon$$

$$\ell_2 = \Big[(\varepsilon\varepsilon_1)(\varepsilon_2 k_1) - (\varepsilon k_1)(\varepsilon_1\varepsilon_2)\Big]k_2 + \Big[(\varepsilon k_1)(\varepsilon_1 k_2) - (\varepsilon\varepsilon_1)(k_1 k_2)\Big]\varepsilon_2$$
$$+ (1 \leftrightarrow 2) + \Big[(\varepsilon_1\varepsilon_2)(k_1 k_2) - (\varepsilon_1 k_2)(\varepsilon_2 k_1)\Big]\varepsilon$$

$$\ell_3 = \frac{1}{2}(\varepsilon_3\varepsilon_4)\Delta - (k_3\varepsilon_4)\varepsilon_3 + (k_4\varepsilon_3)\varepsilon_4 \quad .$$

The vectors Σ and Δ are the sum and the difference of k_3 and k_4, respectively. The denominators D_i follow from the quark and gluon propagators,

$$D_1 = 8x_1\Big[x_3 + x_4 - (k_3 k_4)\Big](k_3 k_4)$$

$$D_2 = 8x_1 x_4 (k_2 k_3) \quad .$$

The amplitude $F_4(1234)$ in which all gluon lines are attached to the heavy quarks (fig. 1a) is a bit more involved. Writing

$$F_4(1234) = -\frac{1}{4}\,\frac{H(1234) + 2x_4\, H'(1234)}{D_4}$$

we have

$$H(1234) = \Big[A(1234;34) + 2(\varepsilon_3 k_4)\, B(124;4)\Big](\varepsilon k_1) - (k_1 \leftrightarrow \varepsilon_1)$$
$$+ \Big[A(4321;31) + 2(\varepsilon_3 k_4)\, B(421;1)\Big](\varepsilon k_4) - \Big[\varepsilon_4 \to k_4\Big](\varepsilon\varepsilon_4)$$
$$+ \Big[A'(1134;34) + 2(\varepsilon_3 k_4)\, B'(114;4)\Big](\varepsilon\varepsilon_2)$$
$$- A(3214;14)(\varepsilon k_3) - (k_3 \leftrightarrow \varepsilon_3) \quad .$$

The symbols A and B abbreviate the expressions

$$A(1234;34) = (\varepsilon_1 k_3)\left[(\varepsilon_2\varepsilon_4)(\varepsilon_3 k_4) - (\varepsilon_3\varepsilon_4)(\varepsilon_2 k_4)\right] - (\varepsilon_1 \leftrightarrow \varepsilon_2)$$
$$- (\varepsilon_2 \leftrightarrow \varepsilon_3)_{\text{subsequ.}} - (\varepsilon_4 k_3)\left[(\varepsilon_1\varepsilon_2)(\varepsilon_3 k_4) - (\varepsilon_1\varepsilon_3)(\varepsilon_2 k_4)\right.$$
$$\left. + (\varepsilon_2\varepsilon_3)(\varepsilon_1 k_4)\right] - (\varepsilon_4 \leftrightarrow k_4)$$

$$B(123;3) = (\varepsilon_1 k_3)(\varepsilon_2\varepsilon_3) - (\varepsilon_1\varepsilon_3)(\varepsilon_2 k_3) \quad .$$

The indices before the semicolon refer to polarization indices, those behind, to the momentum index. A' and B' follow from A and B, respectively, by replacing $\varepsilon_1 \to k_1$. Defining furthermore

$$R(123;4) = (\varepsilon_1\varepsilon_2)(\varepsilon_2 k_4) - (\varepsilon_1\varepsilon_3)(\varepsilon_2 k_4) \quad ,$$

the remaining term H' is given as

$$H'(1234) = -(\varepsilon k_1)\left[(\varepsilon_1\varepsilon_2)(\varepsilon_3\varepsilon_4) - (\varepsilon_1\varepsilon_3)(\varepsilon_2\varepsilon_4) + (\varepsilon_1\varepsilon_4)(\varepsilon_2\varepsilon_3)\right]$$
$$+ (\varepsilon_1 \leftrightarrow k_1) - (\varepsilon\varepsilon_2)\, R(134;1) + (\varepsilon\varepsilon_3)\, R(124;1) - (\varepsilon\varepsilon_4)\, R(123;1) \quad .$$

D_4 is the product of the denominators in the propagators,

$$D_4 = 8\, x_1 x_4 \left[x_3 + x_4 - (k_3 k_4)\right] \quad .$$

The cross section for $(Q\bar{Q}) \to GGq\bar{q}$ is more compact than for gluon final states. We thus present here the final expression for the probability $\Sigma|\mathscr{T}[(Q\bar{Q}) \to GGq\bar{q}]|^2$, color factors and $[4\sqrt{2}\ \Phi(0)]^2$ removed, and summed over all helicities,

$$\Sigma|\mathscr{T}|^2 = \frac{-\sum c^i_{jk} (m^2)^i\, (qk_1)^j\, (qk_2)^k}{D^2} \quad .$$

m is the invariant mass of the quark-antiquark system, q the 4-momentum of the quark. The coefficients c^i_{jk} are symmetric,

$$c^i_{jk}(x_1,x_2) = c^i_{kj}(x_2,x_1) \quad .$$

The only independent, nonzero coefficients are listed below ($x = x_q + x_{\bar{q}}$).

$$c_{00}^0 = -8\, x_q^2 (x_1 - x_2)^2$$

$$c_{10}^0 = 8\, x_q x (x_1 - x_2)$$

$$c_{20}^0 = -2\, x^2$$

$$c_{11}^0 = 4\, x^2$$

$$c_{00}^1 = 8\left[-2 + 3(x_1x_2 + x_1x + x_2x) - x_1^2x_2^2 - x_1^2x^2 - x_2^2x^2 - 5\, x_1x_2x\right]$$
$$+ 4\, x_q\left[(1 - x_1x_2)(4 - x) - 2\, x^2(2 - x)\right] + 2\, x_q^2\left[3\, x_3(2 - x) - 2 - 6\, x_1x_2\right]$$

$$c_{10}^1 = 2(x_1 - x_2)\left\{\left[1 - x_1x_2 - 2\, x(2 - x)\right] - x_q(2 + x)\right\}$$

$$c_{20}^1 = -1 + 5x - \frac{3}{2}\, x^2 + x_1x_2$$

$$c_{11}^1 = 2(1 - x_1x_2) + x(3x - 10)$$

$$c_{00}^2 = -16 - 11\, x_1x_2x + 14\, x_1x_2 + 31x - \frac{43}{2}\, x^2 + 6\, x^3$$
$$+ x_q\left[4\, x(2 - x) - 4(1 - x_1x_2) - x_1x_2x\right] - x_q^2\left[4 - 3\, x - x_1x_2\right]$$

$$c_{10}^2 = (x_1 - x_2)\left[3 + \frac{1}{2}\, x_1x_2 - 2x + x_q\right]$$

$$c_{20}^2 = -\frac{1}{4}\left[3(2 - x) + x_1x_2\right]$$

$$c_{11}^2 = \frac{1}{2}\left[3(2 - x) + x_1x_2\right]$$

$$c^3_{00} = \frac{1}{8}\left(-26 + 34x - 13x^2 + 2x_1x_2x + 10x_1x_2\right) + \frac{1}{4}x_q\left(x - x_q\right)$$

$$c^3_{10} = \frac{1}{8}\left(x_1 - x_2\right)$$

$$c^3_{20} = -\frac{1}{16}$$

$$c^3_{11} = \frac{1}{8}$$

$$c^4_{00} = -\frac{1}{16}\left(6 + x_1x_2 - 4x\right)$$

$$c^5_{00} = -\frac{1}{64}$$

Finally, the denominator D is given as

$$D = x_1x_2\, m^2\left(m^2 - 2x\right) \quad .$$

These expressions have been obtained by processing the Feynman diagrams through REDUCE and SCHOONSCHIP.

TABLE 1

Fraction of events of a given type which fall into class A, as well as the total class A fraction

m_{cut} =	.001	.01	.1	.2	.3
all events	.09	.21	.30	.31	.25
GGGG events	.09	.22	.33	.30	.25
$GGq\bar{q}$ events	.6	.51	.43	.39	.26

Figure Captions

Fig. 1. Orthoquarkonium decay into GGGG and $GGq\bar{q}$.
Permutations of gluon lines are not shown.

Fig. 2. Orthoquarkonium decay into γ + GGG and γ + $Gq\bar{q}$.
Permutations of photon and gluon lines are not shown.

Fig. 3. Decay amplitude for a quarkonium state ($Q\bar{Q}$) to some final state F.

Fig. 4. Magnitude of the 4-jet cross section in onium decays as a function of the invariant mass cut of 2-jet bundles. Separately shown are the GGGG final states with and without 3G vertex, and $GGq\bar{q}$ final states for five "light" quark flavors.

Fig. 5. Distribution of the minimum invariant mass of 2-jet bundles, normalized to the (Born term) decay width in units of α_s/π.

Fig. 6. Minor distributions of the various 4-jet decay modes.

Fig. 7. Distribution of the energy difference between the two jets belonging to the minimum mass 2-jet bundle of 4-jet events. (a) minimum mass cut at 1/9, (b) minimum mass between 2/9 and 3/9.

Fig. 8. (a) Kinematical configuration of class A events. The thrust axis coincides with one of the jet momenta. The three remaining jets lie on the opposite side of the plane perpendicular to the thrust axis. (b) Class B events. There are two jets on each side of the plane perpendicular to the thrust axis (which coincides with the sum of the momenta).

Fig. 9. Thrust distributions of the jets 2, 3 and 4 (in fig. 8a) in the rest frame of the recoil system, for invariant 2-jet mass cut at 2/9.

Fig. 10. Energies of the two 2-jet bundles in their own c.m.s. each, for class B events.

Fig. 11. Angular distribution of the jets in the slim bundle relative to the thrust axis in their own c.m.s. for class B events.

Fig. 12. Gluon-jet broadening in $(Q\bar{Q}) \rightarrow \gamma + 2$ jets in the jets' rest frame by gluon bremsstrahlung, paralleled to bremsstrahlung off quarks in the e^+e^- continuum.

Fig. 13. Thrust in the recoil system of photon decays; all parton-parton and parton-photon pairs have mass larger than 2/9.

Fig. 14. Energy difference of the two slow jets in the recoil system, the mass of parton and photon pairings between 2/9 and 3/9.

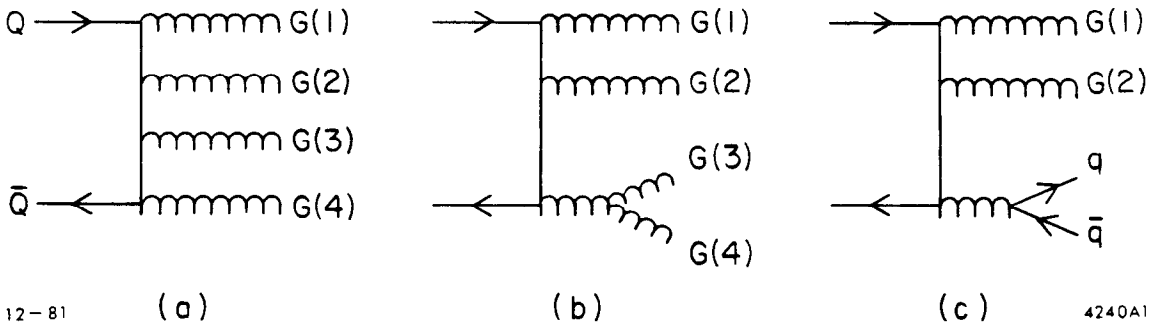

Fig. 1

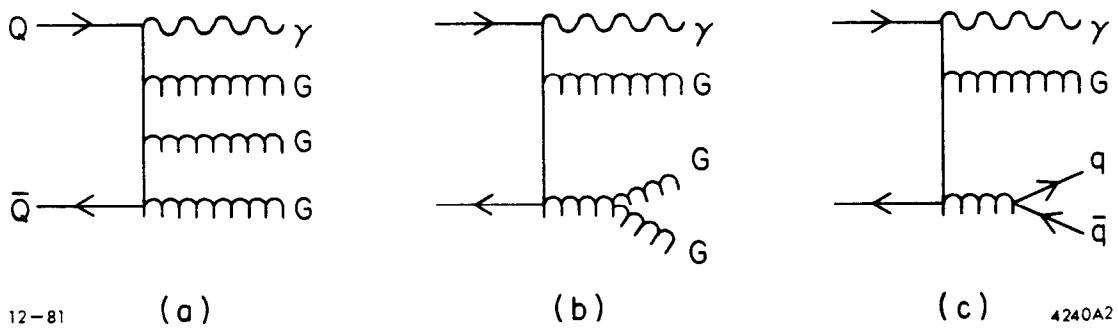

Fig. 2

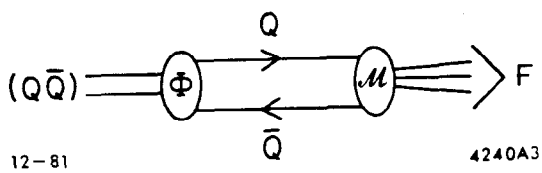

Fig. 3

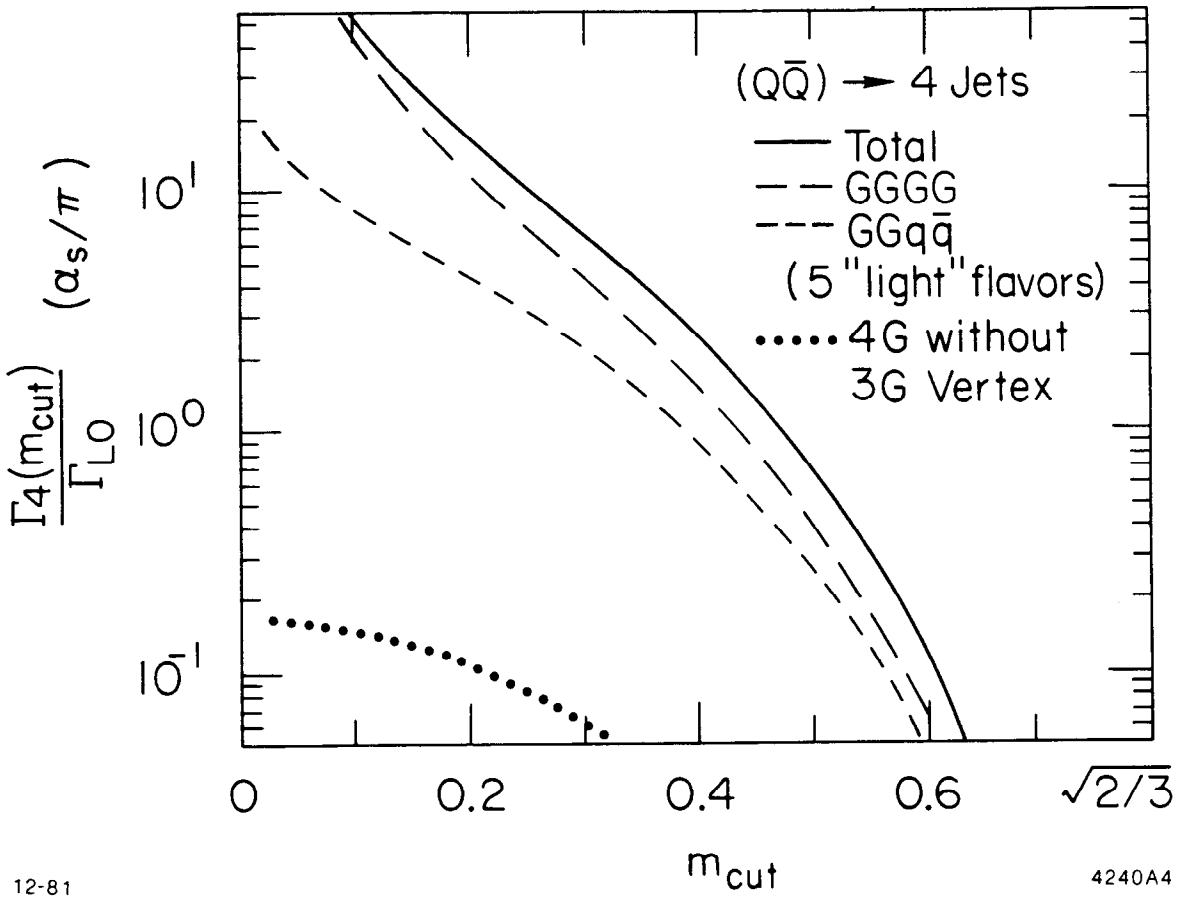
$(Q\bar{Q}) \rightarrow 4$ Jets
Total
GGGG
GGq$\bar{q}$
(5 "light" flavors)
4G without 3G Vertex
$\frac{\Gamma_4(m_{cut})}{\Gamma_{LO}}$ (α_s/π)
10^1
10^0
10^{-1}
0
0.2
0.4
0.6
$\sqrt{2/3}$
m_{cut}
12-81
4240A4

Fig. 4

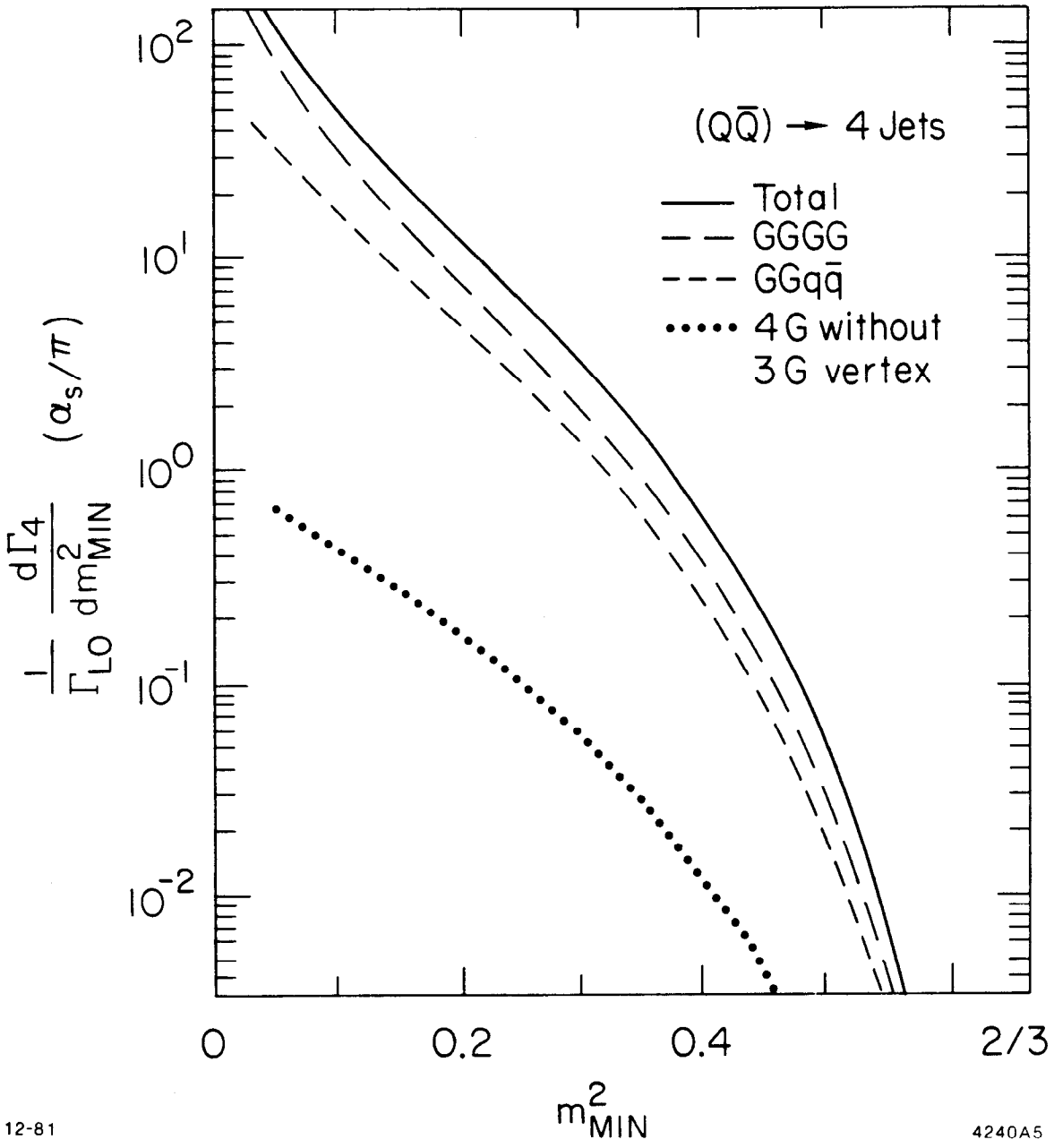
$(Q\bar{Q}) \rightarrow 4$ Jets
Total
GGGG
GGqq̄
4G without 3G vertex
$\frac{1}{\Gamma_{LO}} \frac{d\Gamma_4}{dm^2_{MIN}} (\alpha_s/\pi)$
10^2
10^1
10^0
10^{-1}
10^{-2}
0
0.2
0.4
2/3
m^2_{MIN}
12-81
4240A5

Fig. 5

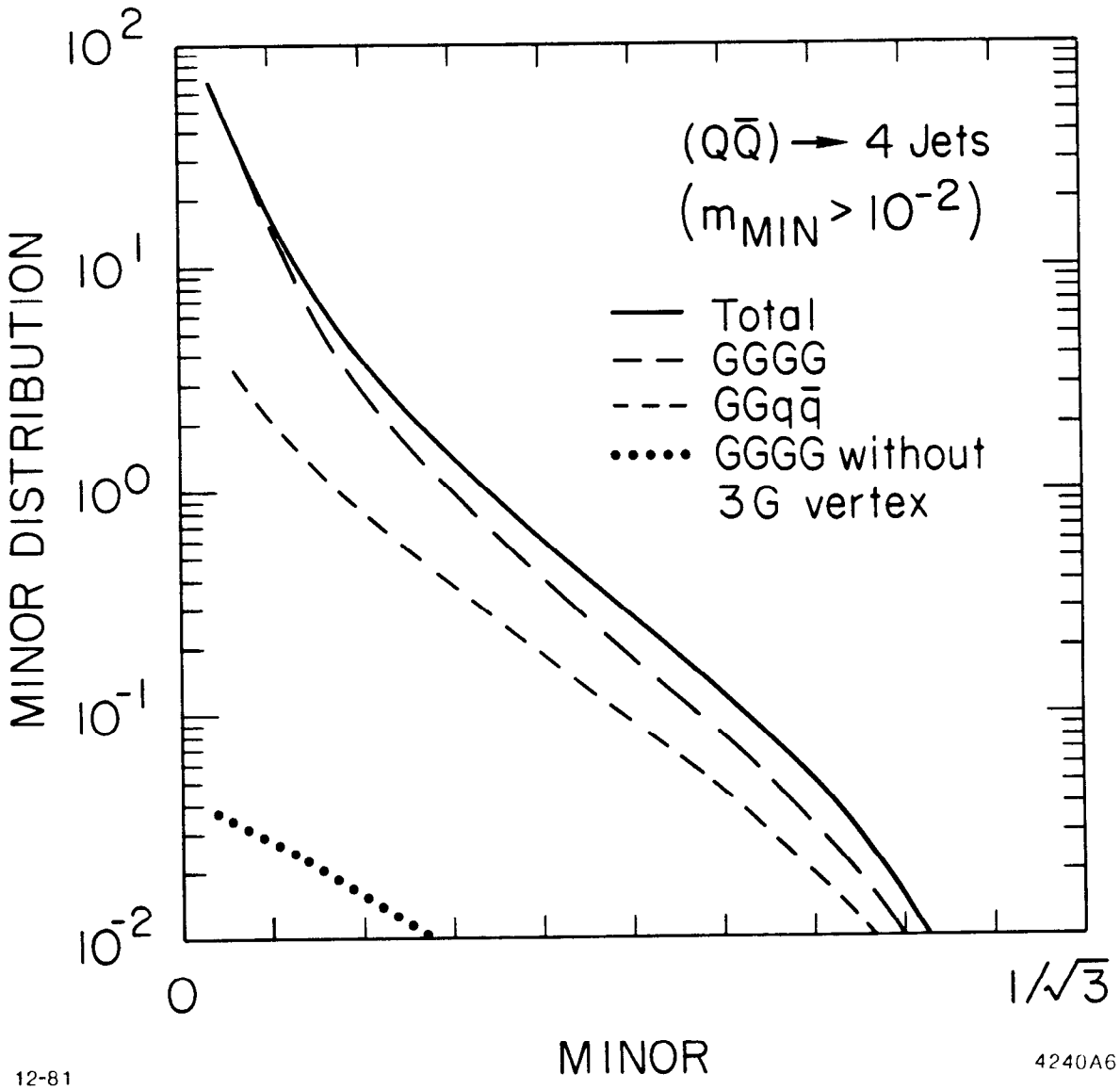
10^2
10^1
10^0
10^{-1}
10^{-2}
MINOR DISTRIBUTION
$(Q\bar{Q}) \rightarrow$ 4 Jets
$(m_{MIN} > 10^{-2})$
Total
GGGG
GGq$\bar{q}$
GGGG without 3G vertex
0
$1/\sqrt{3}$
MINOR
12-81
4240A6

Fig. 6

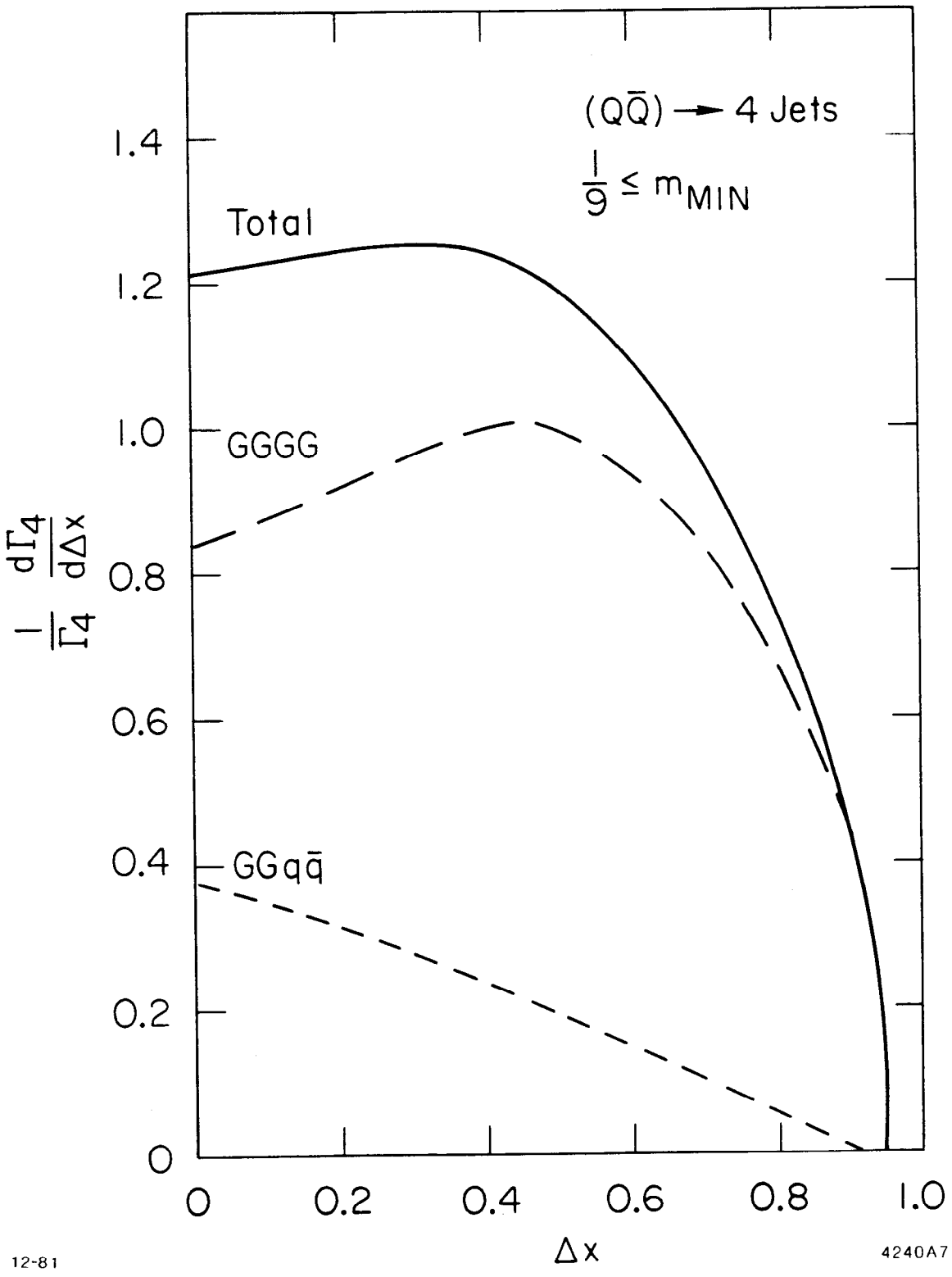
$(Q\bar{Q}) \rightarrow$ 4 Jets
$\frac{1}{9} \leq m_{MIN}$
Total
GGGG
GGq$\bar{q}$
$\frac{1}{\Gamma_4}\frac{d\Gamma_4}{d\Delta x}$
Δx
0
0.2
0.4
0.6
0.8
1.0
1.2
1.4
12-81
4240A7

Fig. 7(a)

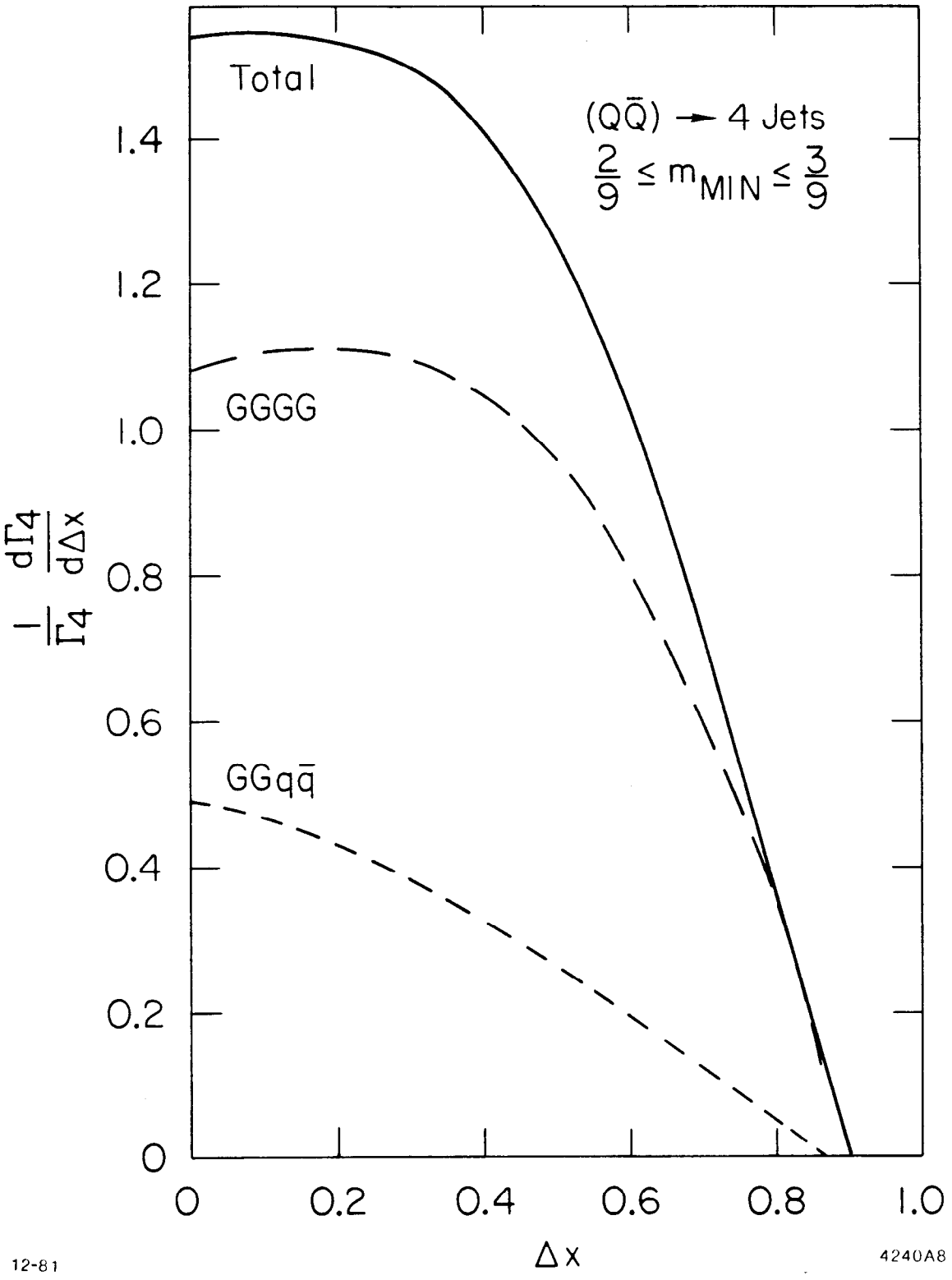
Total
$(Q\bar{Q}) \rightarrow 4$ Jets
$\frac{2}{9} \leq m_{MIN} \leq \frac{3}{9}$
GGGG
$GGq\bar{q}$
$\frac{1}{\Gamma_4}\frac{d\Gamma_4}{d\Delta x}$
0
0.2
0.4
0.6
0.8
1.0
1.2
1.4
0
0.2
0.4
0.6
0.8
1.0
Δx
12-81
4240A8

Fig. 7(b)

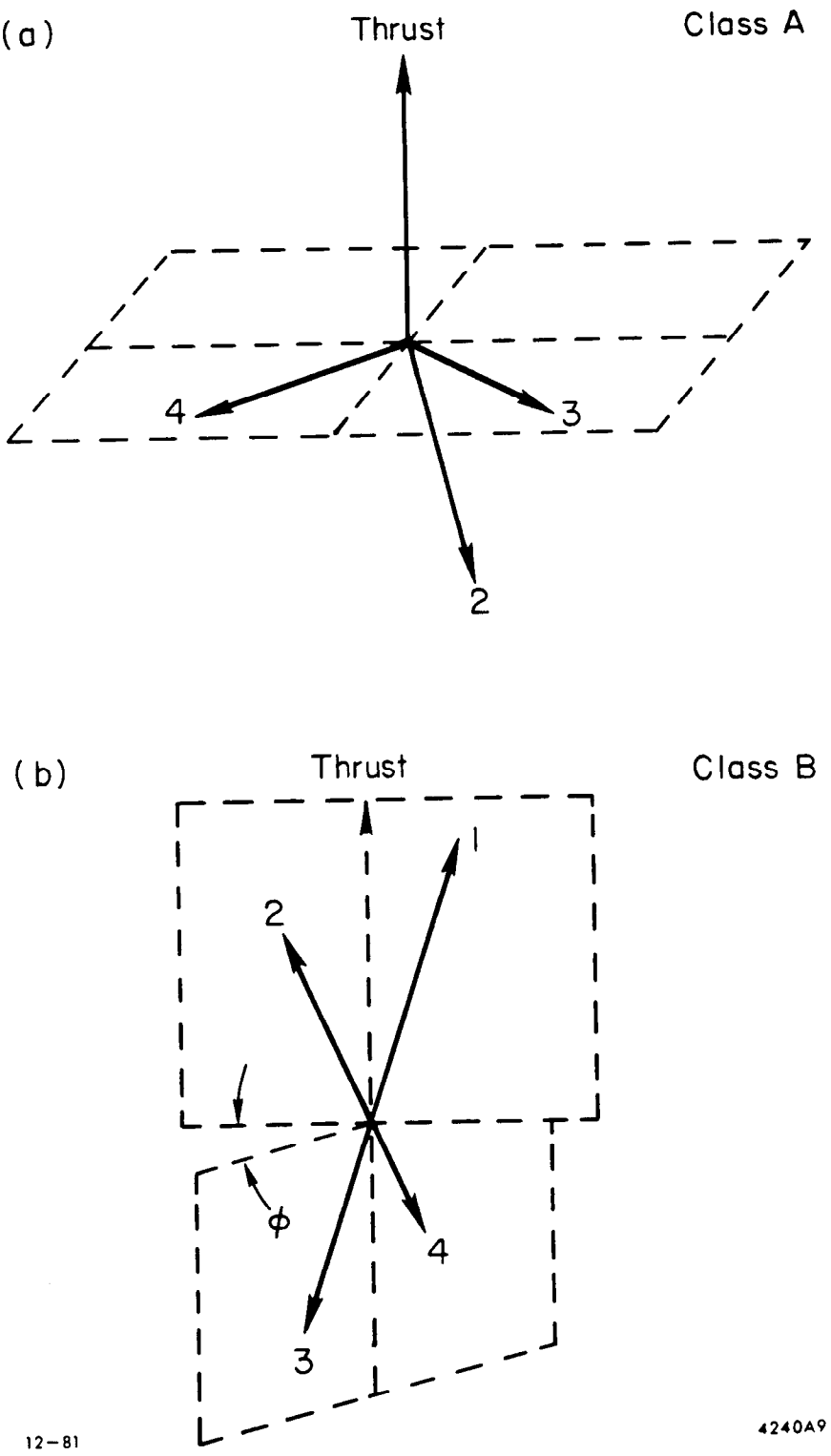

Fig. 8

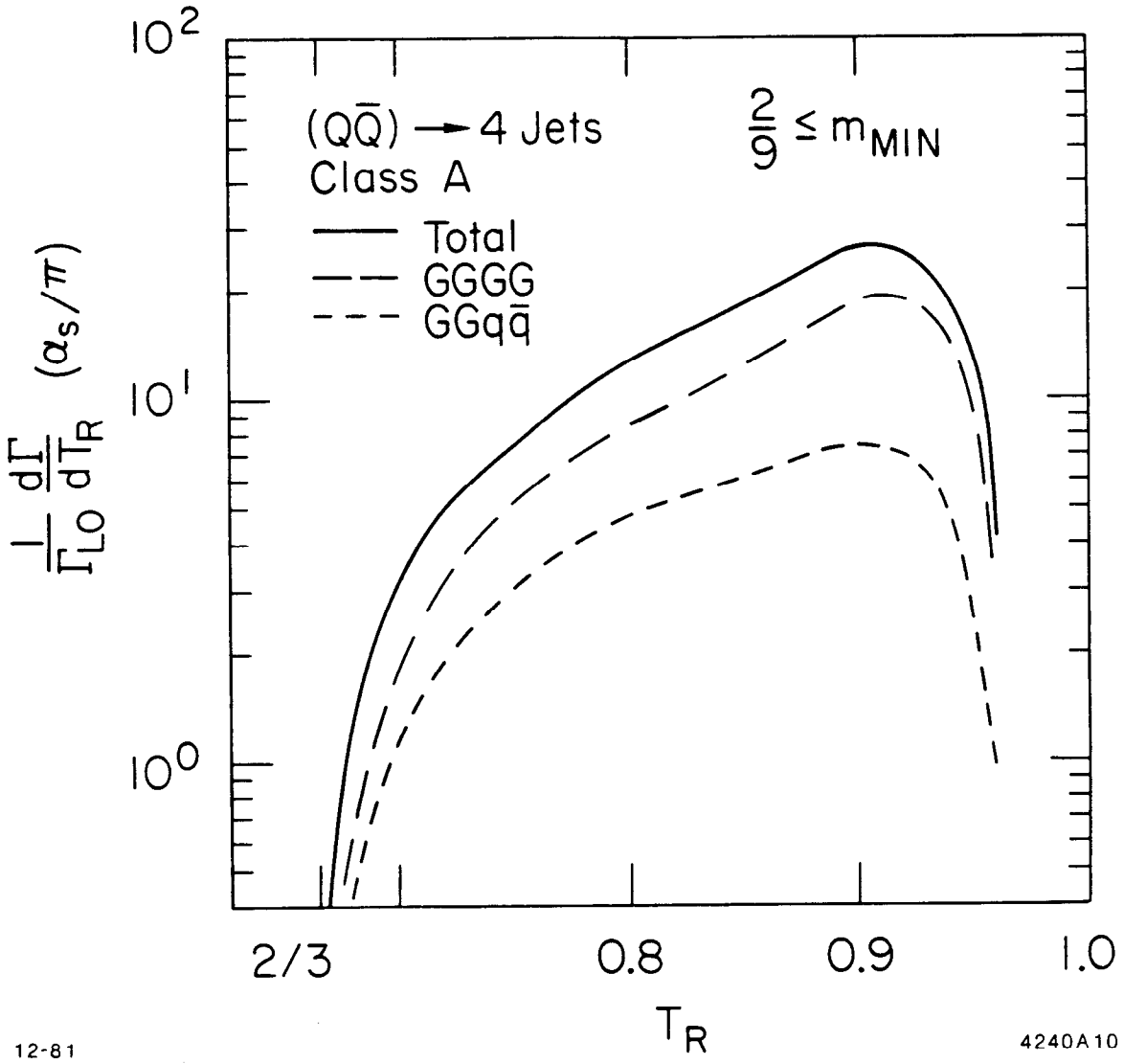
10^2
10^1
10^0
$(Q\bar{Q}) \rightarrow 4$ Jets
Class A
$\frac{s_{16}^2}{9} \leq m_{MIN}^2$
Total
GGGG
GGq$\bar{q}$
$\frac{1}{\Gamma_{LO}} \frac{d\Gamma}{dT_R} \; (\alpha_s/\pi)$
2/3
0.8
0.9
1.0
T_R
12-81
4240A10

Fig. 9

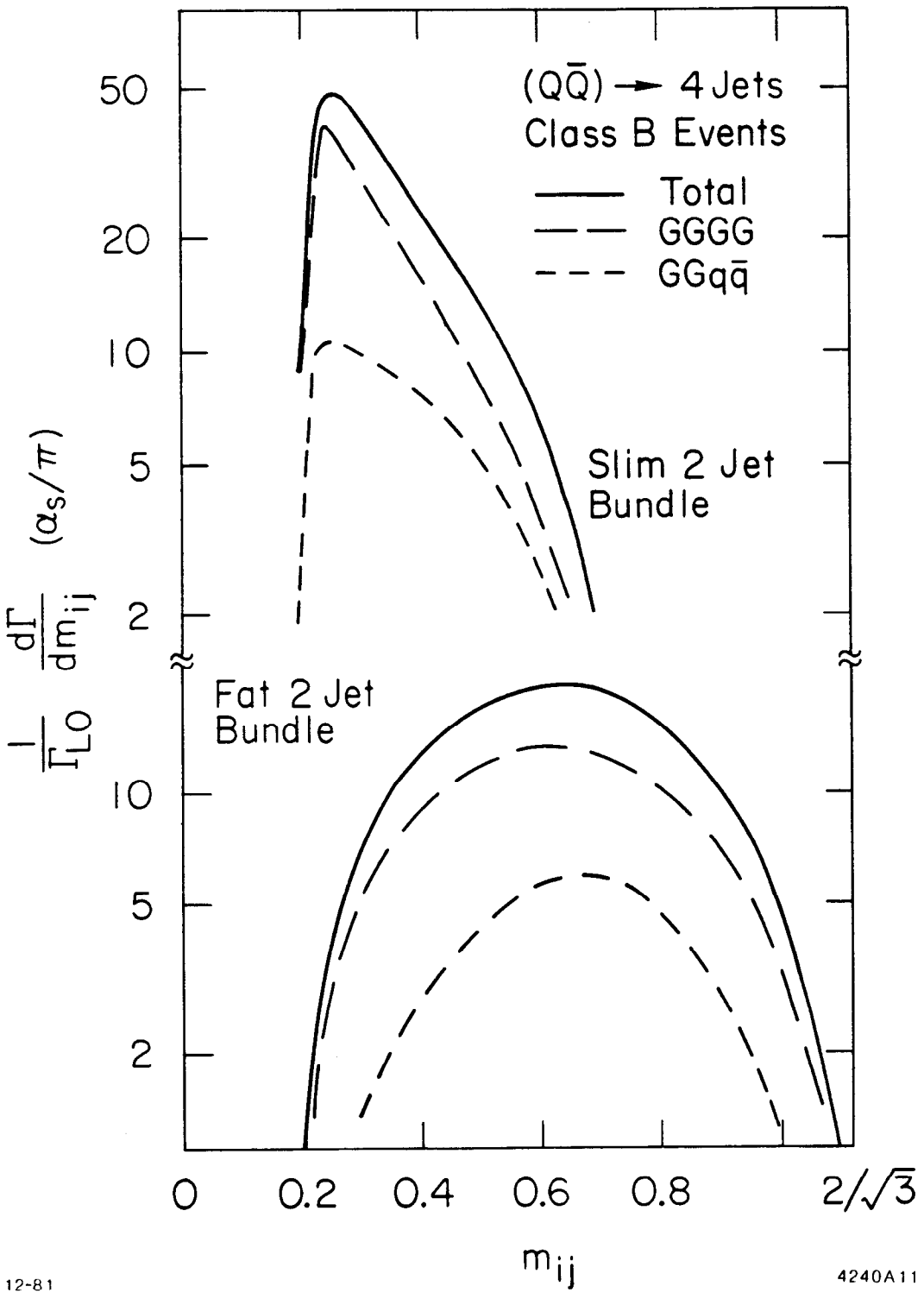
$(Q\bar{Q}) \rightarrow$ 4 Jets
Class B Events
Total
GGGG
GGqq̄
Slim 2 Jet Bundle
Fat 2 Jet Bundle
$\frac{1}{\Gamma_{LO}} \frac{d\Gamma}{dm_{ij}} (\alpha_s/\pi)$
50
20
10
5
2
10
5
2
0
0.2
0.4
0.6
0.8
$2/\sqrt{3}$
m_{ij}
12-81
4240A11

Fig. 10

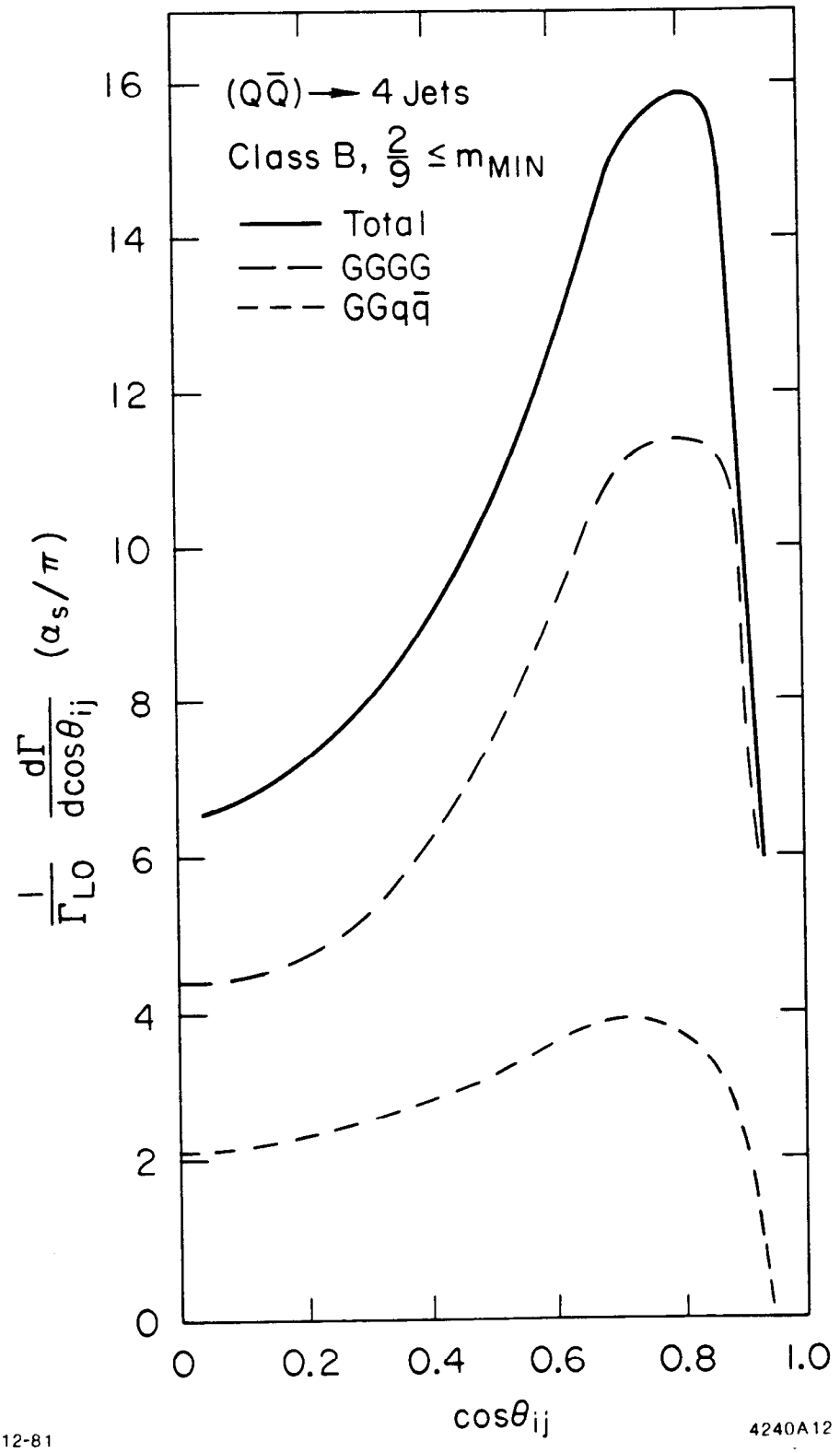
$(Q\bar{Q}) \rightarrow$ 4 Jets
Class B, $\frac{2}{9} \leq m_{MIN}$
Total
GGGG
GGq$\bar{q}$
$\frac{1}{\Gamma_{LO}} \frac{d\Gamma}{d\cos\theta_{ij}} (\alpha_s/\pi)$
$\cos\theta_{ij}$
0
2
4
6
8
10
12
14
16
0
0.2
0.4
0.6
0.8
1.0
12-81
4240A12

Fig. 11

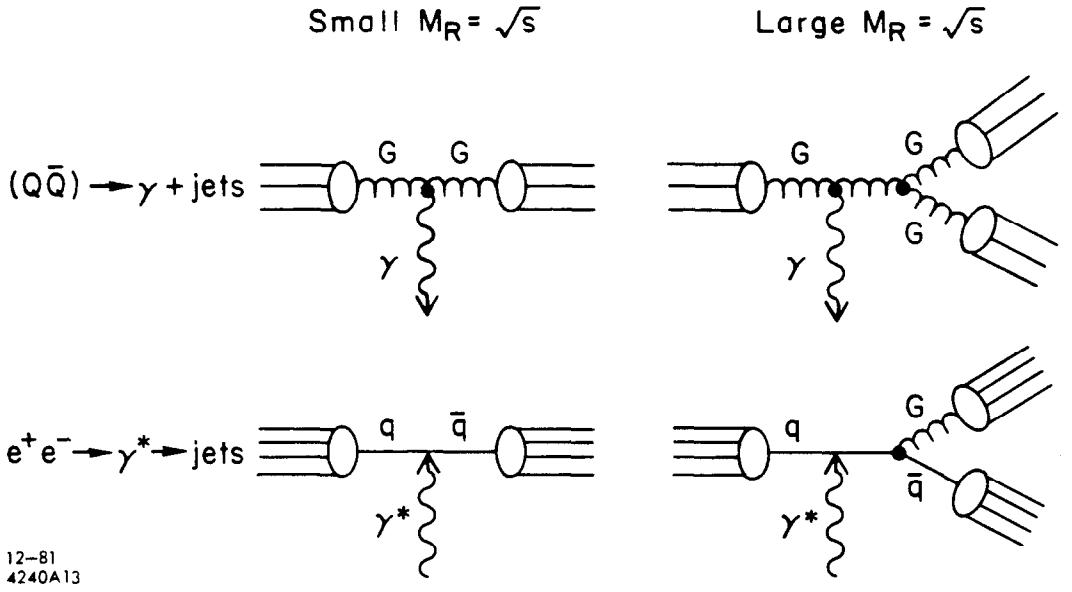
Small $M_R = \sqrt{s}$
Large $M_R = \sqrt{s}$
$(Q\bar{Q}) \rightarrow \gamma$ + jets
G
G
γ
G
G
G
γ
$e^+e^- \rightarrow \gamma^* \rightarrow$ jets
q
$\bar{q}$
γ^*
q
G
$\bar{q}$
γ^*
12–81
4240A13

Fig. 12

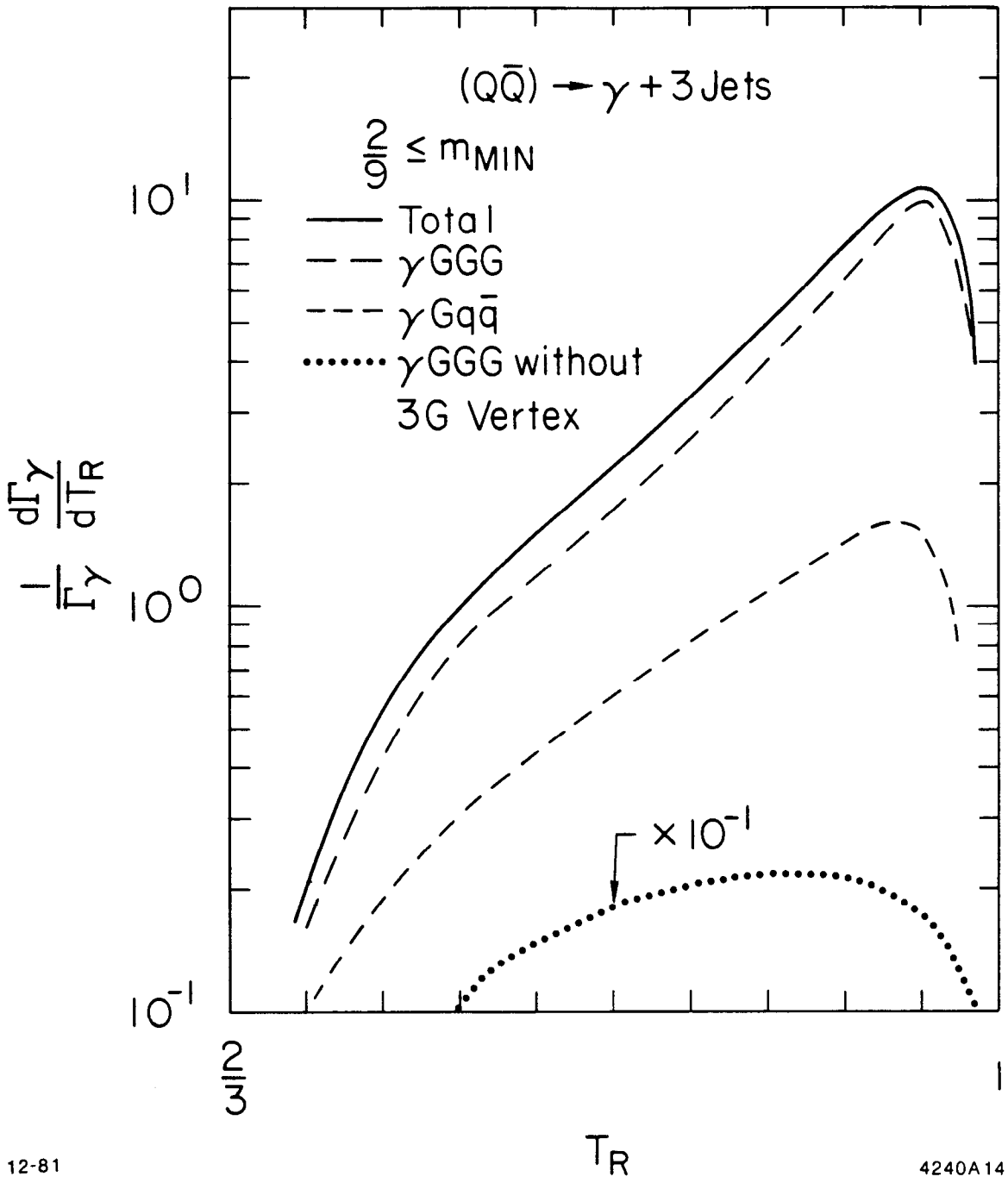
$(Q\bar{Q}) \rightarrow \gamma + 3$ Jets
$\frac{2}{9} \leq m_{MIN}$
Total
γGGG
$\gamma Gq\bar{q}$
γGGG without 3G Vertex
$\times 10^{-1}$
$\frac{1}{\Gamma_\gamma} \frac{d\Gamma_\gamma}{dT_R}$
10^1
10^0
10^{-1}
$\frac{2}{3}$
1
T_R
12-81
4240A14

Fig. 13

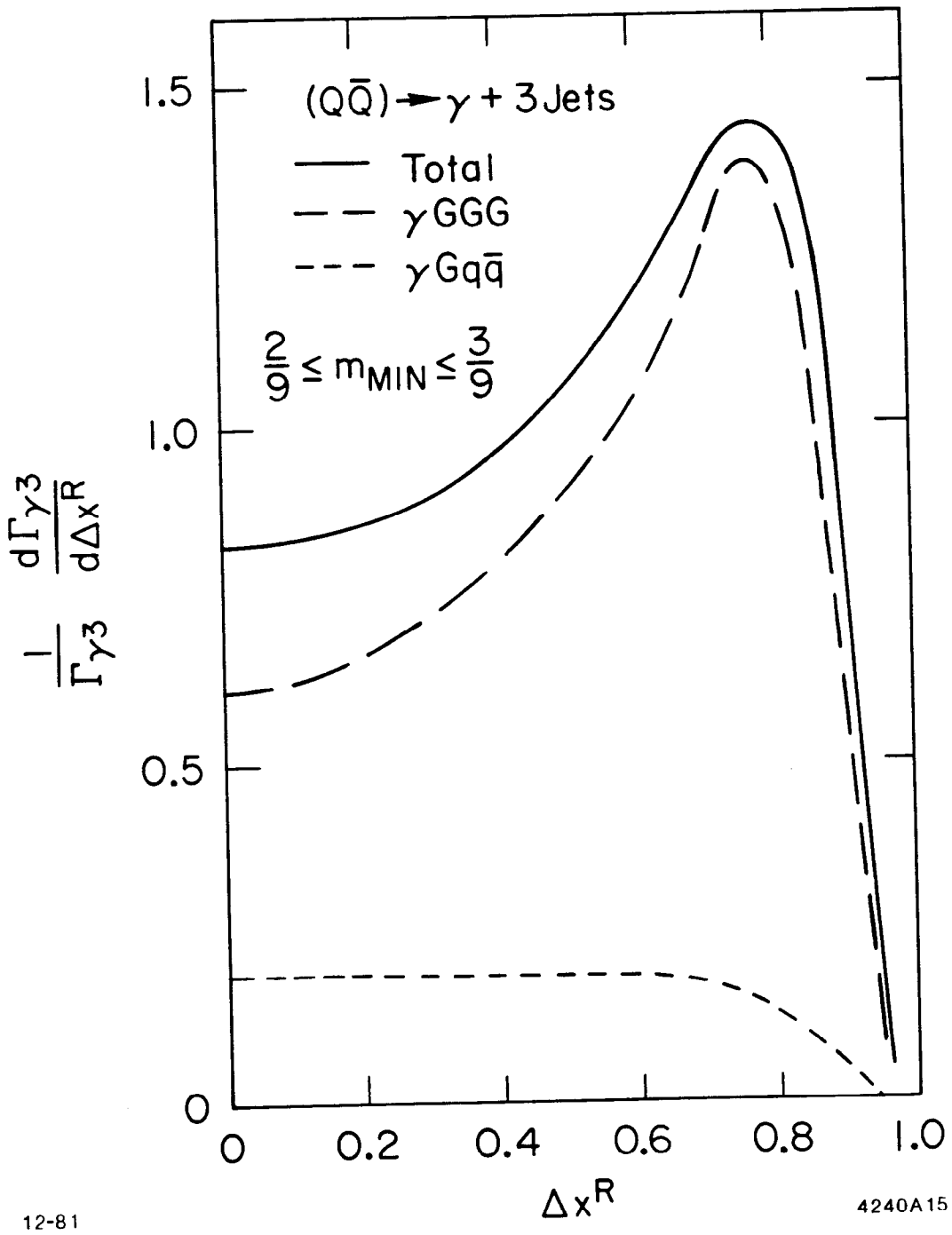
$(Q\bar{Q}) \rightarrow \gamma + 3$ Jets
Total
γGGG
$\gamma Gq\bar{q}$
$\frac{2}{9} \leq m_{MIN} \leq \frac{3}{9}$
$\frac{1}{\Gamma_{\gamma 3}} \frac{d\Gamma_{\gamma 3}}{d\Delta x^R}$
1.5
1.0
0.5
0
0
0.2
0.4
0.6
0.8
1.0
Δx^R
12-81
4240A15

Fig. 14